Fusing Terahertz and Mid Infrared Technologies to Recycle E-waste Black Plastics

by

Anand Sandagdorj

A thesis

presented to the University of Waterloo

in fulfillment of the

thesis requirement for the degree of

Master of Applied Science

in

Electrical and Computer Engineering

Waterloo, Ontario, Canada, 2022

Author's Declaration

I hereby declare that I am the sole author of this thesis. This is a true copy of the thesis, including any required final revisions, as accepted by my examiners.

I understand that my thesis may be made electronically available to the public.

Abstract

Plastic is a unique material, it is lightweight, resilient, non-reactive, waterproof, and low-cost. Due to its versatility and use in everyday products and consumption, it has become a huge environmental concern. In 2015, it was reported that 381 million tonnes of plastic waste were produced, black plastics making up 15% and the electronics industry contributing 20% from e-waste.

Currently there is no effective sorting technology to sort black or very dark colored plastics as they absorb most of the probing energy. Therefore, they cannot be sorted or recycled and end up in landfills. To solve this problem, a new technique must be established.

In this thesis, we propose the use of Terahertz (THz) and Mid-Wave Infrared (MWIR) Spectroscopy with machine learning algorithms to interpret and identify different types of e-waste black plastics. Each black polymer material that interacts with terahertz and MWIR rays affect the shape of the spectrum and has a unique spectral signature. Thus, combining terahertz with MWIR spectroscopy to get multidimensional sensory data will allow us to train a classification model identify black plastics with high accuracy while mitigating the shortcomings of both technologies.

Acknowledgements

It has been a memorable learning and reflective experience for me as a young adult and marked the beginning of my professional career. This experience would not be possible without the help of those who have supported and cheered for me during my journey from the start to finish. I would like to take this opportunity to personally name and thank these incredible people.

Firstly, I would like to thank all my supervisors, Safieddin Safavi-Naeini, Hamid Karbasi and Hamed Majedi for their relentless guidance, professional insight, and consultations in assisting me making the right decisions and allowing me to always rely on them when I needed direction. They have showed me the support of academic community and really encouraged my research, giving me the chance to work on a project that I am proud of.

I would also like to extent my gratitude to Daryoosh Sadaeekia, Arash Rohani and Adam Sanderson. They have been incredible professionals and it was an honor to work alongside them through this project. They helped me deal with so many technical difficulties in their free time and always willing to lend hand. They have my utmost respect and appreciation with them.

I would like to thank my family and friends, as well as my partner for standing by my journey and showing all supports that I ever could ask for. All these people have been an inspiration for my work and my driving point to succeed. Thank you all.

Lastly, I would like to thank WEEE lab at Conestoga College, TeTechS Inc., and CIARS lab at University of Waterloo for letting me use their space and equipment. For the development of the terahertz-based sorting system, I would like to thank everyone that have helped during development, Sevan Sirin, Serdar Salci, Michael Wright, Abhishek Vyas, Parvathy Santhosh Kumar, Mehdi Fadaie Tehrani, Abdul Rehman and Brandon Harkness.

Table of Contents

List of Figures

List of Tables

Chapter 1
Introduction

1.1 Background

Plastic is a unique material, it is lightweight, resilient, non-reactive, waterproof, and low-cost. Due to this, its use in e-waste has increased in types and quantity. It's over-consumption and versatility in everyday use poses a major environmental concern. Plastic pollution has become a significant environmental issue as the rapid increase of plastic products far outweighs the world's ability to deal with them. In 2015, it was reported that 381 million tons of plastic waste are produced [1], 20% of which comes from e-waste [2] and 15% are black plastics which cannot be recycled and end up in landfills [3].

There are multiple reasons e-waste plastics end up in landfill. First, there are inconsistent regulations regarding e-waste recycling. For example, the US and Europe have different definitions of e-waste. In Europe, small household appliances such as refrigerators, microwave ovens, coffee makers and toasters are considered as e-waste, but are not by the US. Even e-waste from nations with strict environmental regulations still continue to be shipped to countries where the environmental regulations are not strict and/or labor is cheaper (e.g., China, India, Pakistan, Nigeria) [4]. Secondly, it is cheaper for manufacturers to use new plastic rather than use recycled due to the higher cost of recycled plastic, as well as not enough regulations and incentives for manufacturers to reduce their use of new plastic [5]. Additionally, recycled plastic that has low purity rate has poor strength and stiffness, exhibiting nonlinear behavior and deformation before failure due to lower interfacial adhesion [6]. Thus, there are no high demand for recycled plastic.

Waste Electrical and Electronic Equipment (WEEE) plastic contains a wider array of hazardous chemicals such as brominated flame retardants (BFRs). Environmental impacts and human exposure can arise from soil and water contamination from nearby recycling and moulding facilities due to these chemicals. BFRs are a group of different substances that are used in many polymers to prevent fire hazards. However, most of them are not fixed to the polymer by chemical binding and therefore leak into the surrounding environment [7]. The chemical structure of BFRs make them persistent in the environment and can be found present in air, wildlife and, in adults and infants [8]. Studies have shown that BFRs have potential adverse affects on central nervous and reproductive systems [9], [10]. Current plastic recycling processes are not designed to remove chemical additives.

The presence of BFRs in recycled plastic can be the result of polymer mixing and contamination during the recycling process. Hence, plastics with BFRs additives are re-introduced into the plastic recycling loop, meaning these additives can seep into other sensitive plastic products (e.g., food packaging and toys). Acrylonitrile butadiene styrene (ABS) and high-impact polystyrene (PS) are of most concern as they are commonly used in electric and electronic equipment and contain the highest concentration of BFRs [11]. Therefore, these plastic types require proper identification and sortation before recycling.

1.2 Current Sorting Technology

One of the biggest challenges in recycling e-waste plastic is sorting them for processing into raw materials. For proper recycling, plastics must be sorted by polymer [12]. Current plastic sorting technology uses Short Wave Infrared (SWIR) cameras [13]. SWIR hyperspectral scanners cover 1000 to 2500 nm on the spectral band and are ideal for detecting light colored plastics. They illuminate light on plastics that are to be sorted, then read the spectral signature of the reflected light from the plastic. Different plastics have different signatures, and they are sorted based on their unique spectral signature. The drawback of SWIR based sorting is that it cannot sort black or very dark colored plastics because dark colors tend to absorb most of the illuminated light and reflect almost nothing back [14]. This leads to black plastics ending up in landfills or incinerated.

1.3 Literature Review

E-waste plastic identification/sortation with both terahertz and MWIR technology is a relatively untouched subject. However, there are multiple studies characterizing materials with terahertz spectroscopy as well as studies utilizing SWIR spectroscopy for non-black plastic characterization with machine learning classification models.

1.3.1 Terahertz Characterization of Materials

Terahertz is a frequency band that falls between far infrared and microwave on the electromagnetic spectrum. The properties of terahertz radiation can be used to investigate solid and chemical structures. Terahertz waves can penetrate objects like plastic, and it is non-destructive and safe [15]. Due to major advancements that have brought down the cost and size of the instruments, it has enabled terahertz technology to be used in industrial settings [16]. Most materials and compositions have distinct fingerprints in the terahertz spectrum. Terahertz time-domain spectroscopy

(THz-TDS) has been shown to be useful for distinguishing pharmaceuticals [17], cancer cells [18], explosives [19] and biohazards [20]. Additionally, THz-TDS has been used to study different polymer types, successfully extracting its unknowns such as the thickness, the absorption coefficient and refractive index [21], [22].

1.3.2 Infrared Spectroscopy and Material Classification

Infrared spectroscopy is the analysis of infrared light interacting with matter. It can be done by measuring the material absorption, emission, and reflection. It is primarily used to determine functional groups of molecules by measuring the vibrations of atoms. The range of infrared wavelength is 700 nm to 1mm, and are usually classified into three regions, near infrared (700-2500nm), mid infrared (2.5-25μm) and far infrared (25μm-1mm) [23]. By analyzing the infrared spectrum, one can identify unknown materials, extract information on the quality of a sample and determine the chemical components present in a mixture. By illuminating infrared light on a sample and measuring the absorption or reflectance of the light at each wavelength, the infrared spectrum is obtained with corresponding frequency of absorbed radiation. All material that interacts with infrared rays will display characteristic vibration frequencies and information about its molecular structure on its measured spectrum. Due to the high information of infrared spectroscopy, it is a very powerful tool for substance identification. There are many studies that have successful uses of SWIR (1-2.5μm) hyperspectral imaging on different type of materials such as plastic, glass and metal, combined with identification techniques like deep learning [14], [24], support vector machines (SVMs)[25] and partial least squares-discriminant analysis (PLS-DA)[26]–[28] that have very high classification accuracies (above 90%). However, these studies do not include e-waste black plastics as SWIR range does not have enough spectral features on black materials to be identified.

1.3.3 Prior Art

A previous research project at WEEE lab at Conestoga College, already dealt with sorting e-waste black plastic samples with a Mid-Wave Infrared (MWIR) hyperspectral camera. Hyperspectral cameras analyze wide spectrums of light instead of assigning primary colors like red, green, and blue to each pixel. The captured light at each pixel is broken down into many spectral bands that provide high information on what was imaged. The processed hyperspectral image from the camera is a unique signature of an object as each pixel contains a full spectrum. Thus, providing both spectral and spatial information.

The set up used in the project is the same as they study done by Dr. Tehrani and Dr. Karbasi in [14] but with an MWIR hyperspectral camera with a spectral range of 3-5µm instead of a SWIR hyperspectral camera with a spectral range of 1-2.5µm. The setup can be seen in Figure 2,

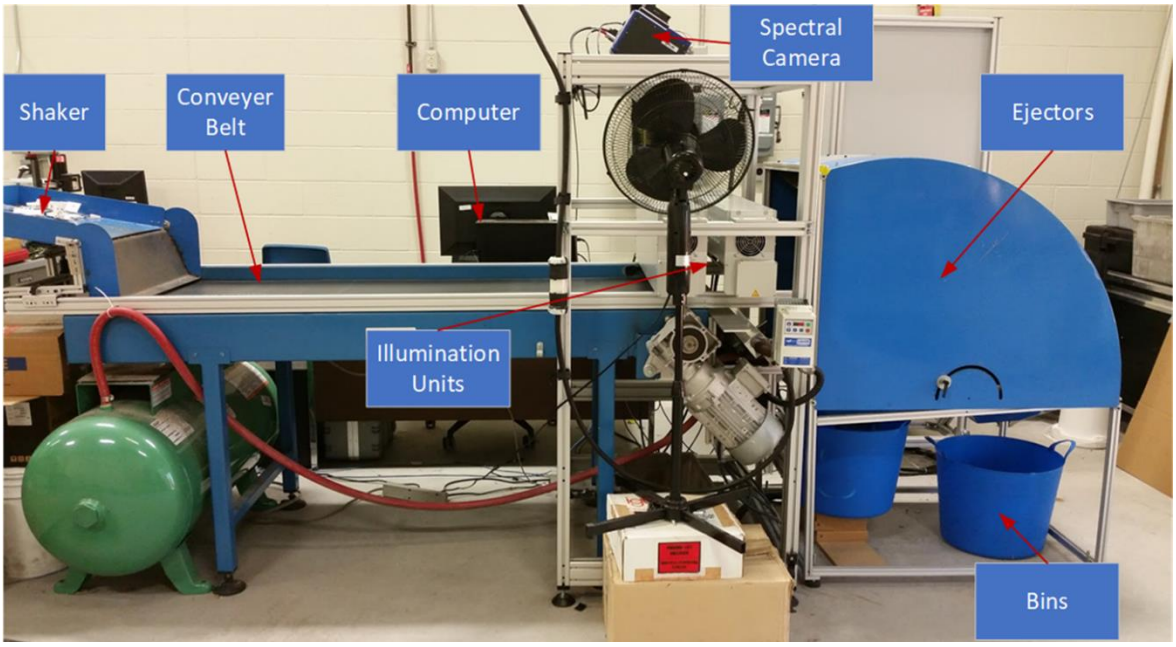

Figure 1: MWIR Sorting Machine

SWIR wavelength is not effective to identify black plastics as the carbon content absorbs most of the probing energy. However, MWIR hyperspectral line-scan on black plastics has enough spectral information to be identified. The MWIR hyperspectral camera had 320 pixels per line and 256 spectral bins. The MWIR hyperspectral camera was integrated into the sorting machine for high-speed sorting. The machine works as follows, 1-inch square black plastic flakes to be sorted are placed on the shaker, which vibrate the plastics to slowly fall on the conveyor belt going at 3m/s. The plastic pieces are flung under the illumination units and exposed to MWIR for a short period of time. The reflected radiation is picked up by the MWIR hyperspectral camera and the spectrum is sent to the computer with a trained shallow neural network classifier. The ejectors then sort ABS from other plastic flakes based on the classifier result into separate bins. The sorting machine is able to sort ABS from PE and PS plastic flakes with more than 80% accuracy in real-time.

1.4 Thesis Objectives

In this thesis, the focus is creating an effective way to identify and sort e-waste black plastics with high efficiency. To achieve this goal, the use of THz spectroscopy and MWIR spectroscopy techniques are discussed. The objective of this thesis is to determine the effective frequency bins in the THz and MWIR regions that characterize e-waste black plastics for real-time applications.

In the THz region the polymers investigated are High-Density Polyethylene (PE), Polycarbonate (PC), Acrylonitrile Butadiene Styrene (ABS), High Impact Polystyrene (PS), Ultra-High Molecular Weight Polyethylene (UHMW), and Polyoxymethylene (POM). In the MWIR region, the polymers investigated are ABS, PS and PE.

We want to establish a method that extract the distinguishable features from both THz and MWIR spectrums of black polymers, combine the multi-spectral data, and simulate a sorting system that identifies different polymers with the multi-spectral data.

1.5 Thesis Organization

This thesis consists of four chapters, background information of e-waste black plastics as well as the current methodologies of dealing with them is described in Chapter 1. The research and development of a sorting system for e-waste black plastic using only THz time-domain spectroscopy is discussed in Chapter 2. The fusion of THz and MWIR spectrums and identifying e-waste black plastic using both techniques is discussed in Chapter 3. Lastly, the conclusion and future recommendations are given in Chapter 4.

Chapter 2
Real-time Terahertz Based Sorting System

The goal of this project is to create a prototype of a real-time terahertz based sorting system capable of identifying falling e-waste black plastic pieces from a stream and eject them based on the plastic type. This chapter will discuss the research and development of the real-time black plastic sorting system as well as the research challenges and results.

2.1 Terahertz Time-Domain Spectroscopy

THz-TDS is a powerful tool for material characterization due to the ability of terahertz radiation to penetrate through objects like plastic, clothing and packaging contact-free [29]. Spectroscopy refers to energy/frequency of photons that pass through or reflect off a sample. For THz-TDS, the time-domain signal directly measures the transient electric field. The terahertz electric field at the receiver is commonly in the range of 10-100V/cm with a time duration of few picoseconds. Since direct electrical detectors have nanosecond to picosecond rise and fall times, it does not have enough resolution to reach sub-picosecond. Therefore, optical techniques with ultrashort optical pulses (less than 100 femtoseconds) are used. For measuring the time-domain of an unknow terahertz field, a femtosecond (fs) laser pulse beam splits along two paths to the THz transmitter and the receiver. The terahertz field is obtained only when the optical laser pulse arrives simultaneously with the terahertz pulse. Since the optical pulse is significantly shorter than few picoseconds and the THz receiver is only sensitive when the split pulses arrive at the same time to the sensors, then the terahertz field can be measured as a function of time. The measured signal is the terahertz field power at single point in time. To measure terahertz field at all time points an optical delay is introduced. As the fs laser pulse is split into two beams, one beam is used to generate the terahertz radiation and the other goes to a path that has adjustable temporal delay, commonly by a high precision stepper motor (stage) with micrometer resolution. The TDS set up can be seen in Figure 1.

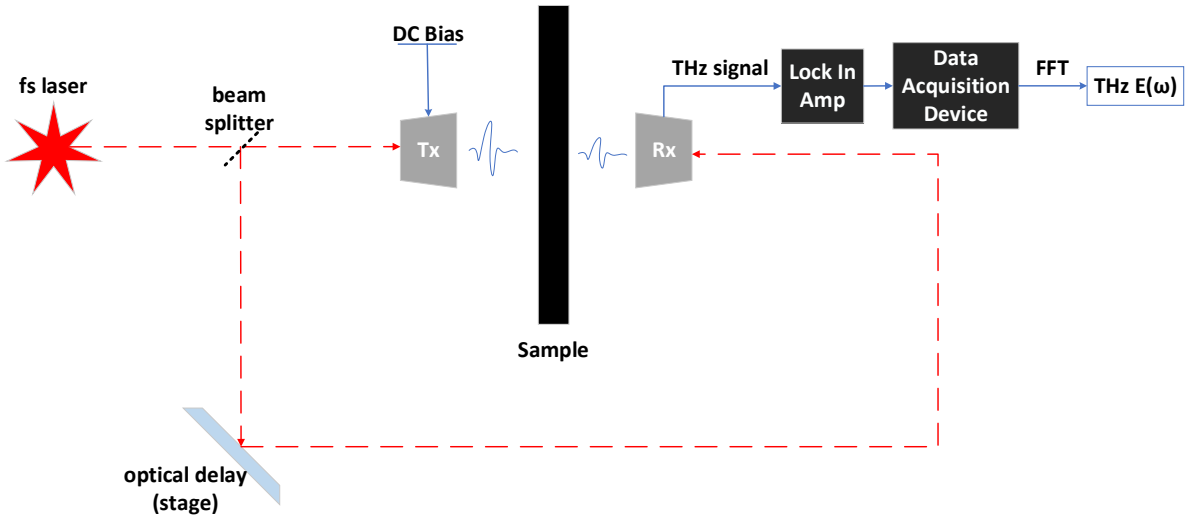

Figure 2: Simplified THz-TDS transmission setup

Moving the stage allows for measuring the THz field at all time points and by adjusting the speed of the stage, higher or lower sampling resolution can be achieved. Higher resolution can be achieved by moving the stage slower but would take a longer time to finish a measurement. While lower resolution can be achieved by moving the stage faster and measurements would be achieved quicker.

2.2 System Overview

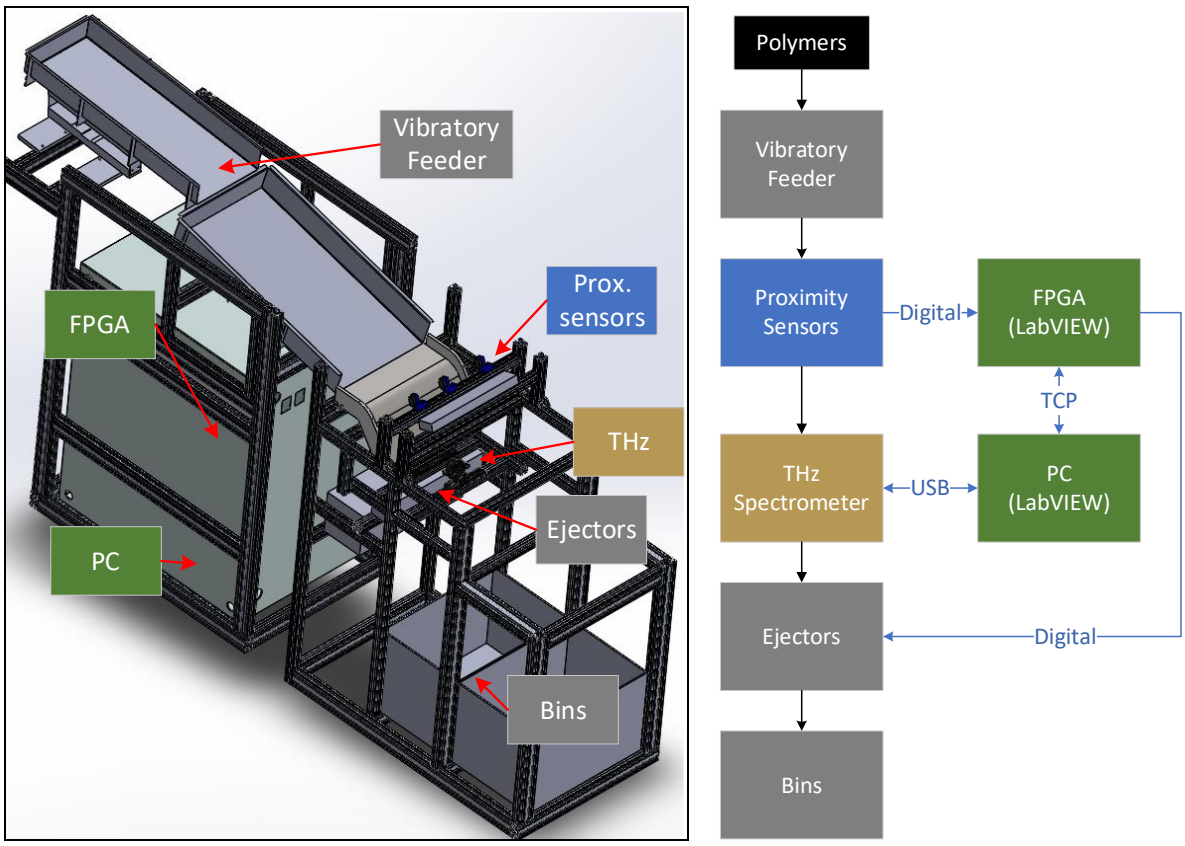

Figure 3: System Overview

The system is similar to the MWIR sorting machine mentioned in Chapter 1, 1-inch black plastic flakes to be sorted are placed on the shaker. The shaker vibrates and gradually slide the pieces to be detected by proximity sensors before they fall in between THz sensors. When the plastic pieces are falling, a THz-TDS spectrometer takes the spectrum of the falling pieces and determines the type of plastic with a neural network algorithm. The neural network is a shallow fully connected network trained from multiple time-domain signals of different black plastic samples. The input of the neural network is the time-domain signal of the falling piece, and the output is the determined plastic type. Depending on the returned plastic type from the neural network, the pneumatic valves are either turned on to eject the piece or let it fall through. Thus, sorting into two compartments.

There are four main systems for this project. First, the system development PC that performs data acquisition, analysis, classification, and optical control. Secondly, the FPGA system that reads

the proximity sensors and controls the pneumatic valves. Third, the THz spectrometer that has the components necessary for fast THz-TDS in multiple regions. Lastly, the vibratory feeder system where the plastic pieces are fed into and stream down to be sorted.

2.3 Vibratory Feeder System

2.3.1 Ramps

The vibratory feeder has three ramps where one leads into the other. The top and middle ramp, seen in Figure 4, shake with vibrating motors to slide the plastic pieces down in a steam. To better separate the plastics, the top ramp's inclination is lower than the middle ramp. The third ramp is mounted right after the middle ramp and is a smooth plastic material that is parabolic in shape and helps the plastic pieces gradually enter free fall before it is detected by the proximity sensors.

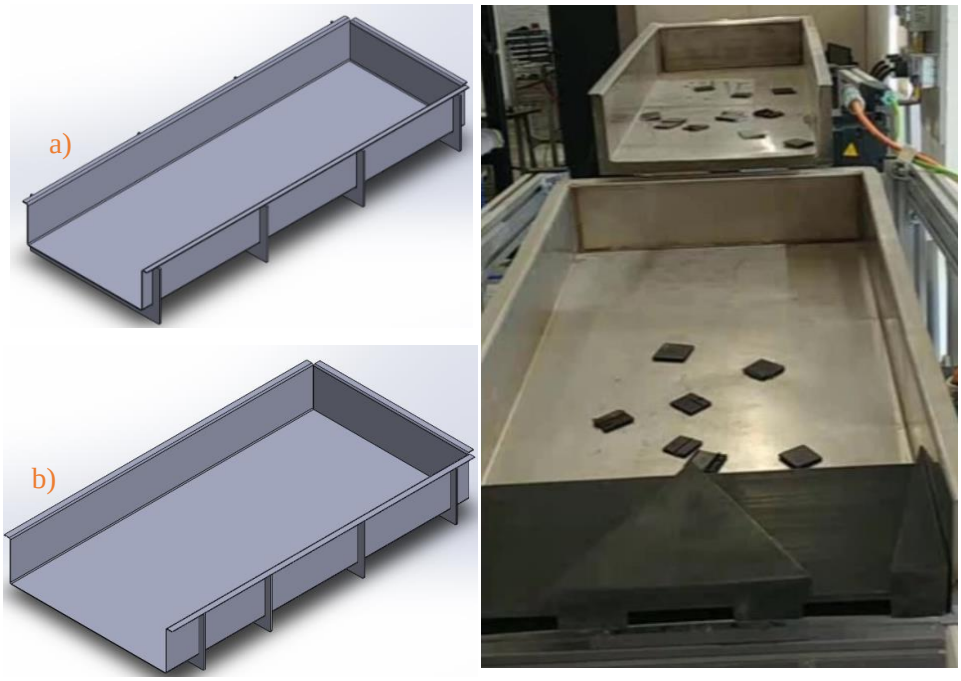

Figure 4: Vibratory feeder ramps, (a) top ramp, (b) middle ramp

2.3.2 Deflectors

The defectors are used as separators for the plastic parts. The parts will slide down the middle ramp and into the deflector, where they will be separated into three streams. This is achieved using two triangles with the tips pointing upwards seen in Figure 6. The deflectors can also be rotated 180

degrees if only two streams are desired instead of three. The plastic parts get separated into three streams as they fall on the third ramp where they will be detected by proximity sensors as seen in Figure 5.

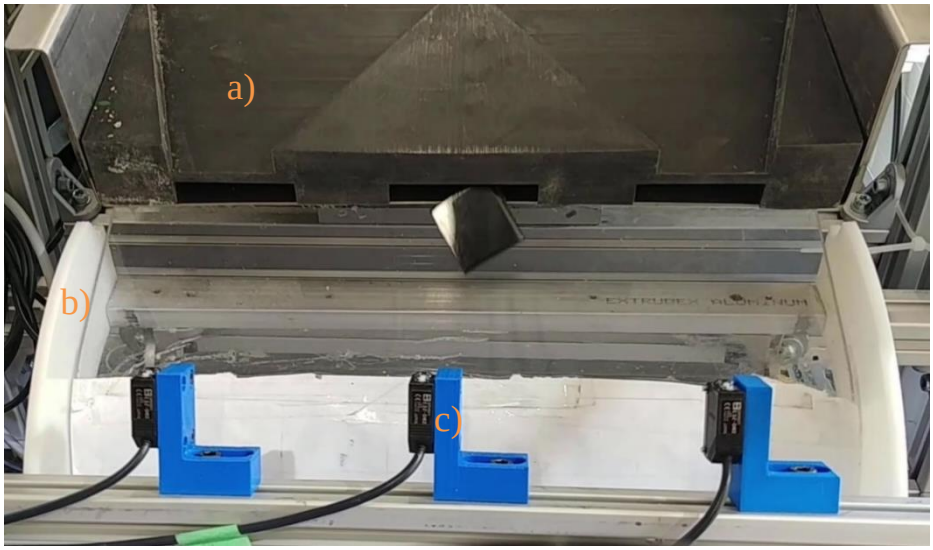

Figure 5: (a) Deflectors, (b) Third ramp, (c) Proximity Sensors

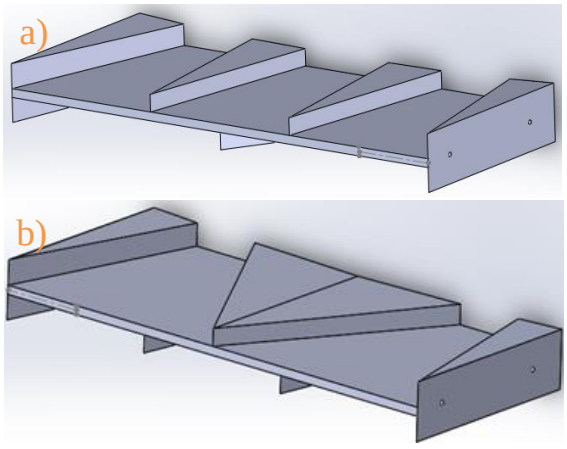

Figure 6: (a) Deflector topside, (b) Deflector underside

There is a bar of aluminum extrusion in front of the third ramp so that the proximity sensors can be mounted to detect the plastic pieces that are sliding down. Beneath the ramp, the terahertz sensors are mounted so that they can detect the plastic parts in free fall. Under the terahertz sensors is the pneumatic valve bank that will blow air onto the plastic parts that need to be ejected from the stream of plastic. On the bottom, there are two collection bins. One collection bin is positioned so that

the falling objects will fall directly into it, while the other collection bin is positioned so that when the air blows the part it will land in the second collection bin.

2.4 Detection and Ejection System

This system's main purpose is to allow for communication between the proximity sensors to the development PC, and the development PC to the pneumatic valve bank. The pneumatic valve actuators and proximity sensors are connected to CompactRIO (cRIO) by National Instruments. The cRIO system provides a real-time operating system and a chassis containing programmable FPGA modules. The cRIO uses a visual programming language that is similar to flow diagrams called a Virtual Instrument (VI). The FPGA system provides precise timing, very little control latency, and high-speed logic which makes it suitable for sorting application. The cRIO detection and ejection system runs a simple algorithm seen in Figure 7, the proximity sensors returns either True or False. If a falling plastic piece is detected it is True and if not, it is False. The three Boolean status is converted to an array (e.g., if sensor 3 is detected and 1 and 2 are not, the array will be 0000 0*100*) and it is sent to the development PC via TCP/IP.

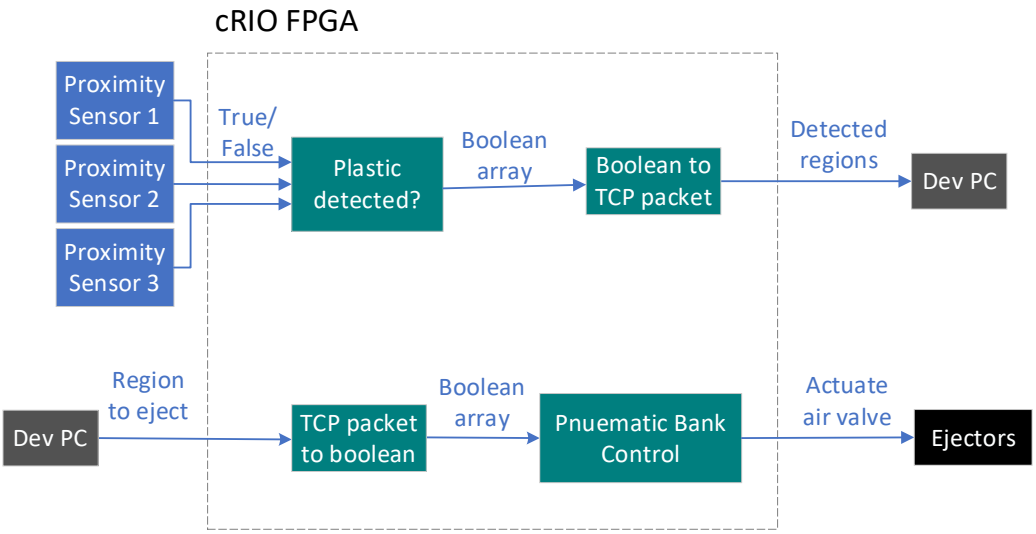

Figure 7: cRIO FPGA Process Flow

Once, the development PC determines if it is a plastic of interest, it will send a Boolean array back via TCP/IP specifying the region to eject (e.g., if the plastic was detected at proximity sensor 3, the returned array will be 0000 0*100*). That region is fed to the pneumatic bank control VI which

actuates the air valves and ejects the falling plastic as seen in Figure 8 and 9 respectively. This process runs indefinitely.

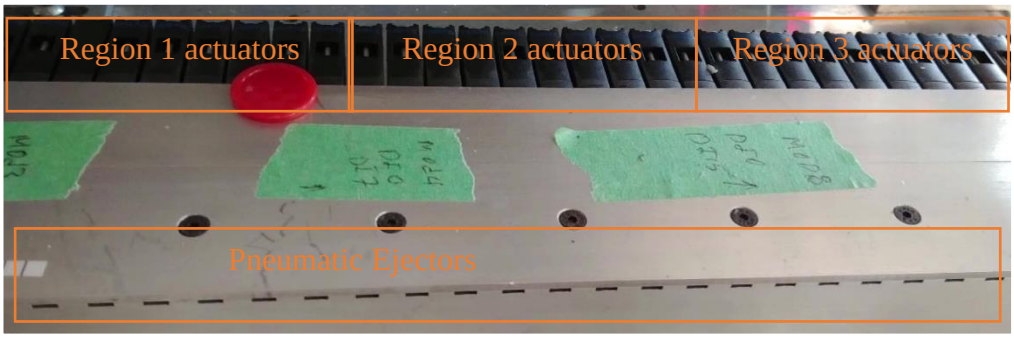

Figure 8: Pneumatic actuators

Figure 9: Plastic ejection

2.5 The Terahertz Spectrometer

The spectrometer used was the Rigel 1550 Spectrometer from TeTechS Inc. It is a portable and compact terahertz time-domain system that is capable of non-destructive material sensing and characterization applications. The transmitter and the receiver are both fiber coupled and have the freedom to be mounted in any test setting as long as they are optically aligned. It has a built in 1550 nm femtosecond fiber laser and a laser beam distribution chassis (more information can be seen in Appendix A). The overall process for scanning falling plastic pieces is seen in Figure 10.

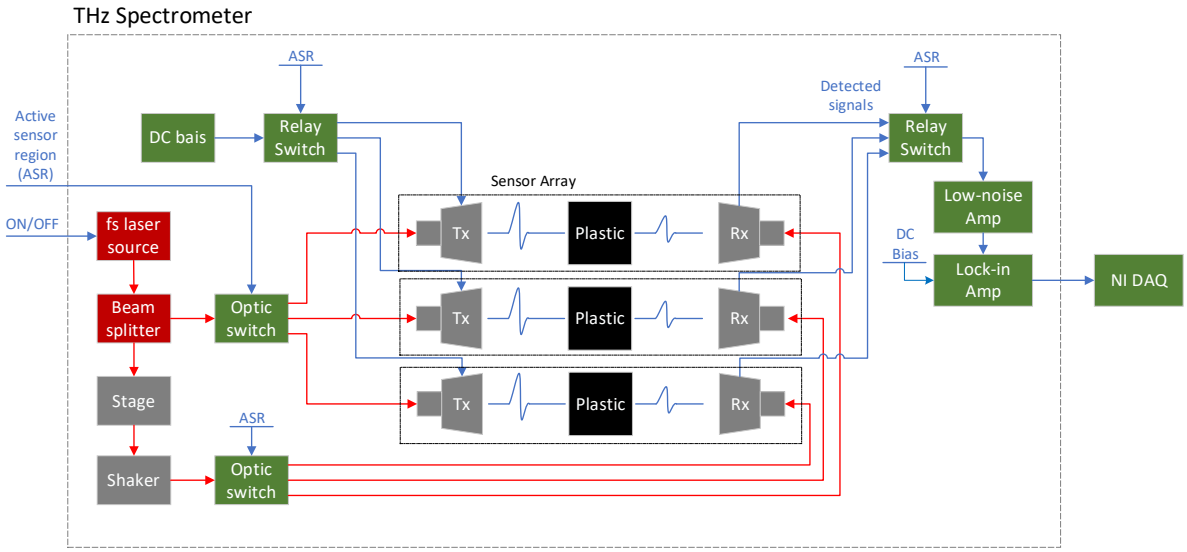

Figure 10: THz spectrometer process flow

The process is as follows: the fs laser is split into two, one for the receivers and the other for the THz generators. The fs laser beam for the transmitter is fed into an optical switch that directs the laser source into a specified sensor head. The receiver beam goes through two optical delay modules before it reaches the optical switch for the receivers. The first optical delay module is a high precision stepper motor (stage) for adjusting the optical delay. The second optical delay module is a voice coil (shaker) that has lower step resolution than the stage but capable of oscillating faster. Both the optical switch for the receiver array and the transmitter array are told which sensor pair must be active from the region detected from the proximity sensors triggered from the Detection and Ejection System. The active pair will receive the transmitter laser beam as well as the delayed receiver beam. The relay switches for the DC bias of the transmitter array and well as the output of the receiver array must to be switched to the same sensor pair before the optical switch. The output of the receiver from the active sensor pair is processed with a low-noise and lock-in amplifiers which are used to avoid unwanted noise and to improve measurement sensitivity. Finally, the output is read by an analog to a digital converter and the digital signal is then sent to the development PC via USB for post-processing.

2.5.1 Femtosecond Laser and Beam Splitter

The femtosecond laser module emits wavelengths in the range of 1550 nm. The output from the laser is given to the power splitter through fiber optics. The power splitter splits in the ratio of

50:50 and the outputs are sent to the transmitter and receiver fiber optic switches. The laser module is connected to the development PC through USB and turned on/off by a laser control VI.

2.5.2 The Stage

The stager is a stepper motor that delays the femtosecond laser by moving in a linear up and down motion. The stepper motor can move at high precision with a minimum size of 0.1µm per step. The stage is used to calibrate and locate the peak of the THz pulse as well as for high resolution scans. The stager must be at the peak of the terahertz signal in order to scan using the shaker. A software application called Zaber is used to move the stage from the development PC via USB.

2.5.3 High Speed Optical Delay Line

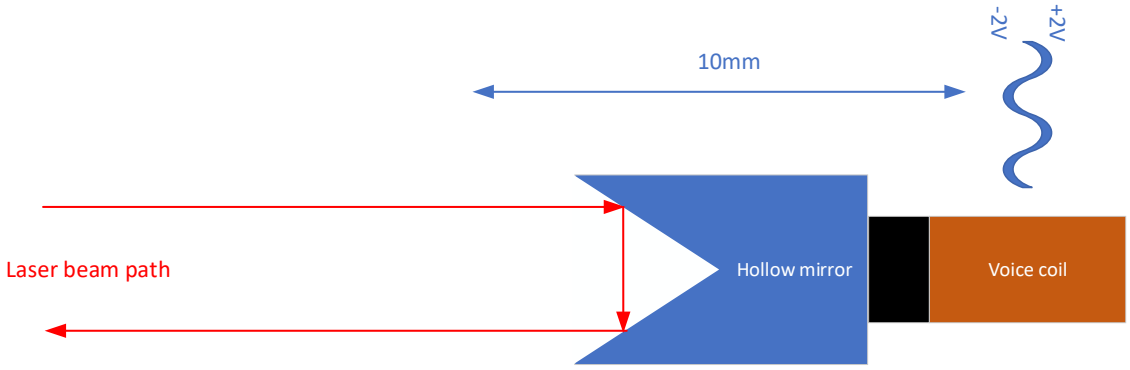

Figure 11: Shaker Module

The high-speed optical delay line (shaker) is a voice coil that delays the femtosecond laser to the receiver fiber switch by moving in a linear motion as seen in Figure 11. It is faster than the stage and capable of real time THz-TDS. It takes -2V to 2V as its input voltage from an NI digital to analog converter (DAC) and has a travel distance of up to 10mm. The NI DAC sends voltage levels following a sine wave. This allows the shaker to delay the fs laser beam up to 20mm. A sine wave is used instead of sawtooth wave that has a linear speed because a sine wave gradually decreases its oscillation speed at its peaks and troughs. This is required when the voice coil is oscillating at high speeds like 80Hz. At high speeds a sawtooth wave would carry too much momentum and cause the shaker to slam to its top or bottom boundaries. The shaker module is controlled by the development PC through the NI DAC.

2.5.4 Fiber Optic Switches

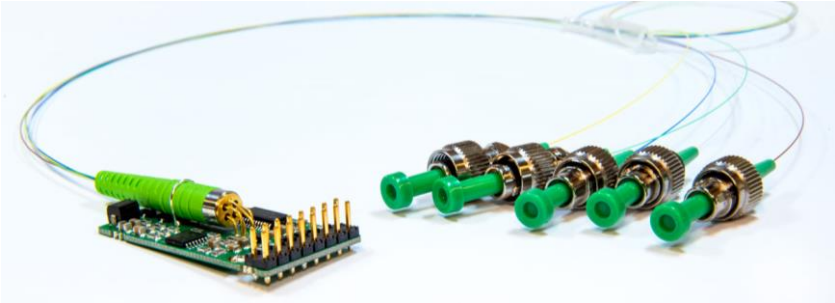

Figure 12: Fiber optic switch [30]

By implementing fiber optic switches to the system, the spectrometer can utilize multiple THz sensor pairs instead of one. This also avoids the need to have expensive fs laser sources and optical delay lines for each sensor pair. The fiber optic switches in use is the Sercalo fiber optic SC1x4 switch. This switch uses micro-electromechanical systems (MEMS) to redirect the input laser source to one of its four ports. The switch has very low insertion loss and low crosstalk between channels (more information can be seen in Appendix B). The switch uses either UART, I2C or parallel interface. For this project, both the switches for the THz transmitter array as well as the THz receiver array are controlled via parallel interface, from the development PC through an NI digital output module. Both the fiber optic switches receive which region to switch to from the development PC. To specify which channel turns on for the laser, three digital input pins on the switches are utilized, PD0, PD1, and PD2. By specifying the digital value (i.e., 5V for 1 and 0V for 0) from a digital output module, there are five states the switches can be in. Each state specifies a channel to direct the laser beam through except for standby mode as seen in Table 1 below.

Table 1: Fiber Switch Active States

Active Channel	PD0	PD1	PD2
Standby	0	0	0
1	1	0	0
2	0	1	0
3	1	1	0
4	0	0	1

2.5.5 Relay Switch Module

The purpose of the relay switch coincides with the fiber optic switches, so that the spectrometer can utilize multiple THz sensor pairs instead of just one. By implementing fiber optic switches to the system, relay switches must also be used for switching the DC bias to the active transmitter and reading the output of the active receiver. The relay switch module for the THz transmitter array has one input channel and eight output channels. The same relay switch design is used for the THz receiver array; eight input channels and one output channel. This module is controlled from the development PC through an NI digital output module. Both the relay switches receive which region to switch to from the development PC. To specify which channel turns on for the DC bias as well as for the active receiver output, eight digital input pins on the switches are used as seen by the ribbon cable in Figure 13.

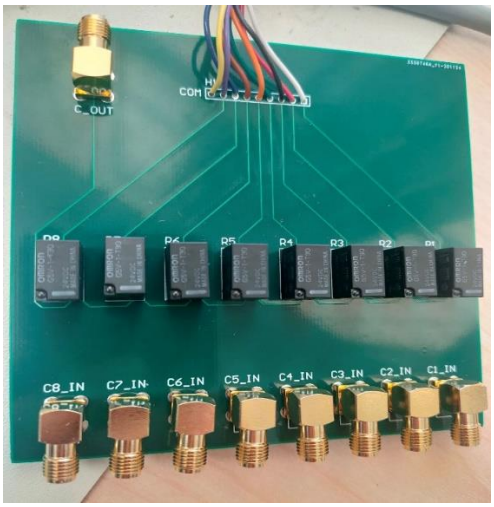

Figure 13: Relay switch for sensor bias and output

The digital output module from the development PC chooses between the eight channels based on the region detected from the Detection and Ejection system. Each channel has a numeric constant which is the binary representation of the selected channel number. The digital output module outputs 24V as 1 and 0V as 0 which latches the relay. For example, to open channel number 3, the binary representation 11111011 or the decimal representation 251 is written to the digital output module. Only one digital output module is used for both relay switches.

2.5.6 Lock-in Detection

The lock-in amplifier is used to measure small signals within a noisy background. The lock-in amplifier selectively amplifies a signal given a reference frequency, in this case, it would be the frequency of the square wave bias signal [31]. The square wave bias is in the few kHz modulation range. The noisy signal coming from the active THz receiver, which is the terahertz time-domain signal, is multiplied by a sine wave at the reference frequency and applied a low pass filter to obtain the DC component. The DC output of the lock-in is read by an analog to digital converter and sent to the development PC via USB.

2.6 System Development PC

The development PC is the 'brains' of the sorting system. It controls all the parameters required for measuring the THz TDS of a falling plastic piece, determining if it is a plastic of interest and communicating to the cRIO to eject or not. The main programming environment used was LabVIEW Real-Time, it is a system application by National Instruments that is used to create and deploy software real-time. It ensures reliable and precise timing for testing, monitoring, and controlling the sorting systems. It uses the same graphical programming language (LabVIEW) as the cRIO. The development PC data flow and processing can be seen in Figure 14.

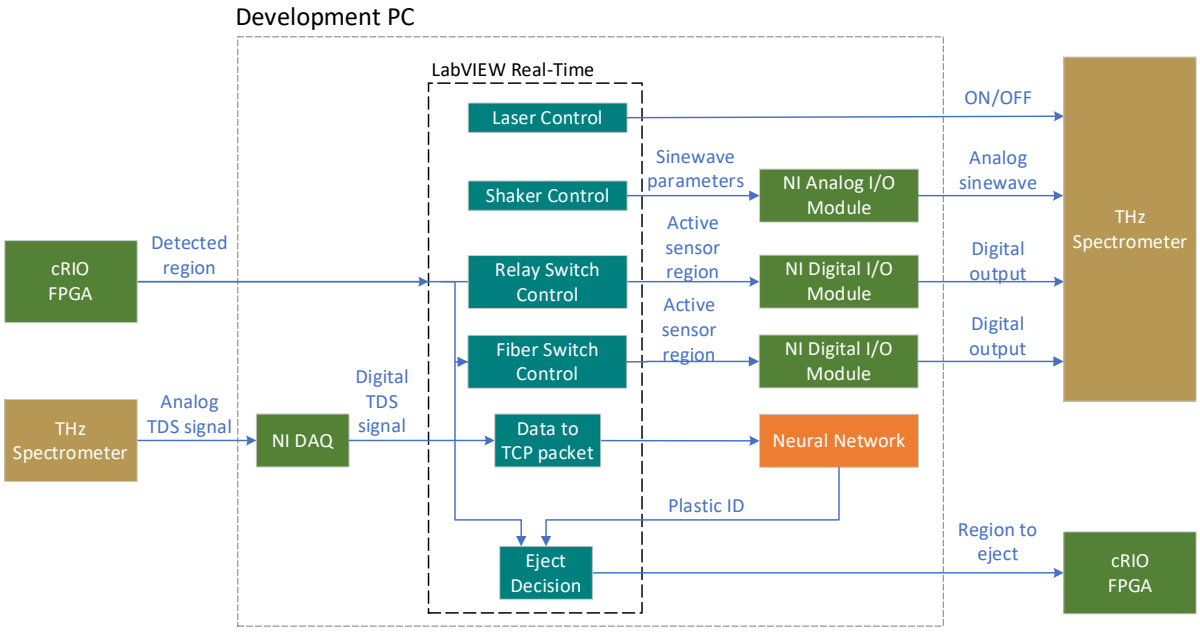

Figure 14: Development PC Process Flow Chart

2.6.1 Optical Initialization

The initialization of the system begins with turning on the fs laser for the spectrometer. This is done by an API that controls the state of the laser. Secondly, the shaker control VI initializes the shaker voice coil by positioning it on its center (at 5mm). After the shaker is positioned, the shaker VI uses an NI DAC to generate a sine wave for the shaker to follow. The voice coil takes -2V to 2V as its input, they correspond to the upper (10mm) and lower (0mm) boundaries of the motor. The shaker VI generates the sine wave parameters for the NI DAC to output. The parameters are the amplitude and frequency of the sine wave. The amplitude corresponds to the optical delay, or the scanning range and the frequency corresponds to the scanning speed of the THz-TDS. Each period the shaker travels from the sine wave input are two scans. From the peak to the trough, and trough to the peak results in two scans per period as seen in Figure 15. The shaker runs indefinitely unless its sinewave parameters must be changed.

2.6.2 Relay and Fiber Optic Switch Control

The PC and cRIO communicate via TCP/IP. Once the proximity sensor has been triggered, the cRIO will signal the PC to optically activate the terahertz sensor pair in the desired region. The region detected and sent from the cRIO is fed into two control VIs, first to the relay switch controller and then the fiber switch controller. Both control modules have a case structure to convert the detected region number, which is an unsigned 8-bit binary number, to the corresponding digital outputs. After the relay and fiber switch controllers turn on the THz sensor pairs in the detected region, the time-domain signal is acquired from the lock-in amplifier.

2.6.3 Time-domain Signal Acquisition

The LabVIEW program that reads the output analog signal of the spectrometer (lock-in amp) uses an NI high speed data acquisition device (DAQ). There are multiple analog scans coming from the spectrometer due to the oscillation of the shaker (up to 80Hz or 160 scans per second). To separate the downward scan from the upward scan of the shaker, the sine wave output from the shaker NI DAC is referenced to trigger the NI DAQ to distinguish where the scans begin and end. The trigger is a digital signal derived from the slope of the sine wave. If the slope of the referenced sine wave is negative, it is scanning the time-domain signal when the optical delay is moving downwards. If the slope is positive, it is scanning the time-domain signal of the upward motion of the optical delay

as illustrated in Figure 15. The time-domain scan of the upward motion is backwards, so it is reversed.

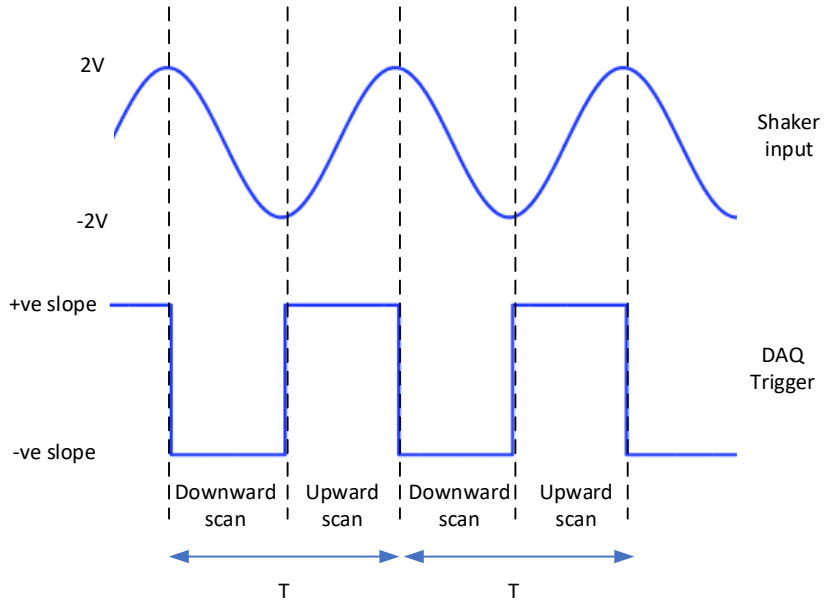

Figure 15: TDS scan trigger from shaker oscillation

2.6.4 Identification

When the NI DAQ acquires a single scan of the time domain signal, it generates a scan number unique to that scan. Both the scan ID and the measured scan are packaged together and sent to a trained neural network for identification via TCP. The neural network is a python script that runs concurrently with the LabVIEW code and determines what type of plastic it is from the received scan. It returns the plastic identification along with the scan ID back to the LabVIEW program via TCP. Once the plastic type and scan ID are received, it determines if the falling plastic is the type to be sorted. If it is a plastic to be sorted, the program determines which region it was detected in from the scan ID and sends that region back to the cRIO. The cRIO will trigger a section of the pneumatic valves to eject the falling part from the stream based on the specified region sent from the PC. If it is not a plastic of interest, the program will not communicate anything to the cRIO and allows it to fall through.

A shallow neural network is used to identify the scan of the plastic. Since the system is heavily time dependent, a simple shallow neural network has advantages in fast data processing and

classification. The shallow neural network contains 3 fully connected layers which reduces the feature size by a quarter at each layer of the network. The structure of the neural network is shown in Figure 16.

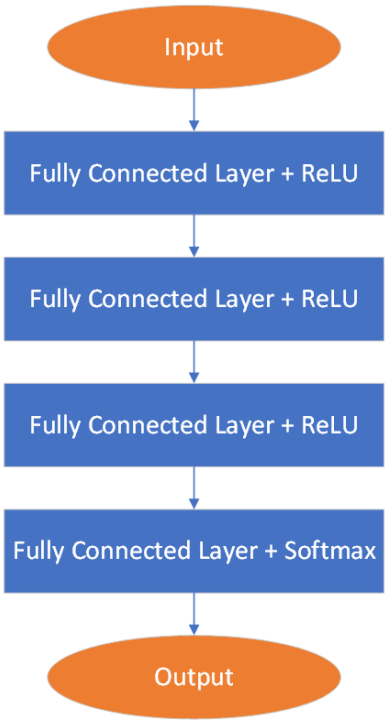

Figure 16: Neural network architecture

In this implementation, the neural network inputs are the time domain signal captured by the NI DAQ which are roughly 310 points. Each point is a 4 bytes floating number which can be sent on one TCP packet for cutting down transmission time. The time domain signal is used instead of the FFT because the shaker at high speeds adds significant amount of noise and has a very small scanning range. Due to these constraints, the time-domain signal was used instead as it still had a significant features to be trained with compared to the FFT signal. Due to the size of this neural network and the small amount of data being processed, it is run on CPU. The CPU processed the neural network at a rate of 65 microseconds per inference.

2.6.5 Training

The network was trained using time domain signals from high impact polystyrene (PS), Acrylonitrile butadiene styrene (ABS), and polycarbonate (PC) plastic sheets with the size of 12 x 12

inch. All the sample plastics had a black coloring and had the thickness of 3.175 mm except for ABS which had thickness of 1.59 mm. The training setup can be seen in Figure 17.

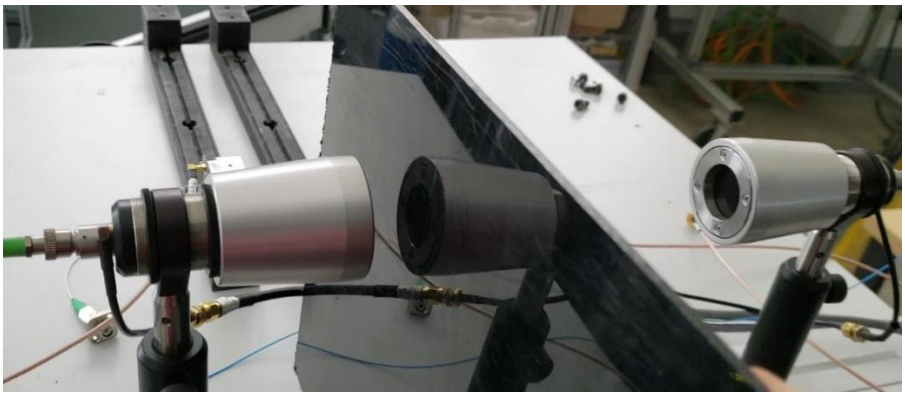

Figure 17: Sample scanning for neural network

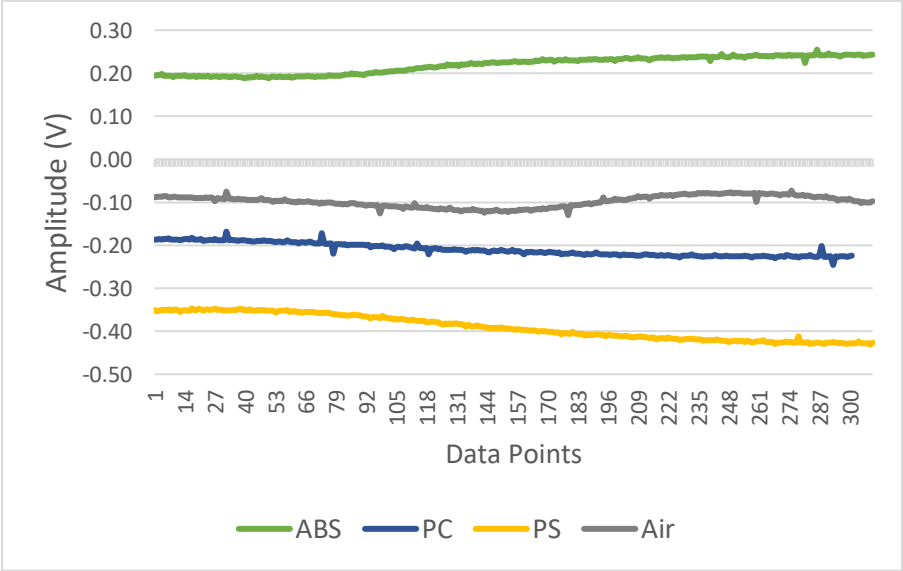

Figure 18: Scan read from NI DAQ with rate of 30 scans per second

The first the neural network was trained using the scan data when the shaker was oscillating at 15Hz (30 scans per second) with the scanning range of 4 mm. Time-domain scan data from the NI DAQ are shown in Figure 18. During training, the signal had random noise added to it to simulate the noisy environment of the sorting system. The network was able to classify these plastics with up to 99% accuracy showing very promising results.

The neural network was later trained with e-waste plastic samples with the size of 1 x 1 inch while the shaker was moving at 40Hz (80 scans per second) with the scanning range of 2.2 mm. The network showed 90% accuracy.

2.7 Implementation and Results

During the development of implementing an array of THz sensor pairs to the sorting line, the current femtosecond laser was not strong enough to generate a viable signal from newly purchased compact THz sensors. A stronger laser source would be required to use the compact THz sensors and unfortunately, there was no budget for a stronger fs laser. Due to this reason, only one sensor pair was implemented which was the THz sensor pair that came with the Rigel 1550 THz spectrometer. Therefore, only single region sorting was implemented as seen in Figure 19. This also meant the relay and fiber optic switches could not be implemented but both modules were working in accordance to their unit tests.

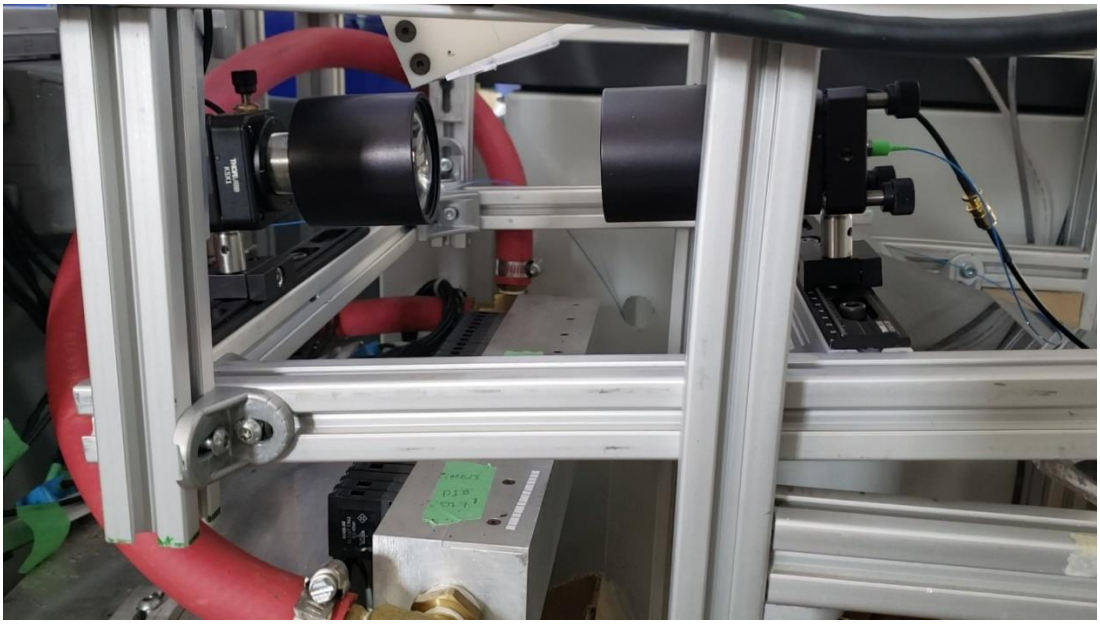

Figure 19: Single THz sensors mounted after proximity sensors and before ejection

The first problem encountered was the THz-TDS signal was very sensitive to the thickness of plastic samples. The thickness difference from e-waste black plastic samples had a significant effect in the time-domain signal, which lowered the accuracy of the neural network. This was due to the similarity and overlapping of the time-domain signal of different plastic samples with little

varying thicknesses. For example, a PS sample with a thickness of 3 mm had a very similar time domain signal as a PC sample with a thickness of 3.175 mm. Due to the limiting scanning range of the shaker, this problem could not be mitigated by increasing the scanning length. The THz sensors were also not sensing the 1x1 inch falling plastic samples at 40Hz scanning rate. The plastic pieces were too small and falling too fast for the spectrometer to capture any scan of it. To overcome these challenges, the thickness of the plastic was controlled to be the same and larger plastic pieces were used. Additionally, only two black plastic samples were used which were PC and PS.

After adjusting the plastic samples, the sorting system was able to identify and eject PC from PS and vice versa. However, many challenges arose from this implementation. First, the plastic samples had to be at least 3 x 5 inches for the THz sensors to be able to detect it. The shaker was moving at its top speed which was 80Hz (160 scans per second) for it to be able to scan a falling plastic piece, identify it, and eject it. As the frequency of the shaker increases, the amplitude (scanning length) must decrease as they are inversely proportional. Moving at its max speed results in a very small scanning range for the THz-TDS and the lock-in amplifier averaging the time-domain signal greatly reducing the features of the THz pulse. Essentially, the real-time THz-TDS sorting system was only looking at a single sub-THz frequency for differentiating the plastic pieces. Scanning a plastic with a single sub-THz frequency in the time-domain results in the spectrometer outputting a flat DC signal, which greatly negate the advantages of the neural network.

Chapter 3
THz and MWIR Fusion

MWIR is a mature technology compared to THz in terms of availability of the cheaper source and detector. MWIR uses frequency domain line scan cameras and measure reflective spectroscopy. They are excellent in detecting and sorting black plastics at high-speed and high throughput but sensitive to surface conditions. Many plastic components that go through the recycling process end up coated in dust or oil. This can cause reflective spectroscopy techniques to detect the spectral signature of the contaminant on the surface of the plastic leading to false classifications. Also, there is very little study done to detect chemical additives such as flame retardant with MWIR.

Terahertz technology on the other hand is still under research and development. Terahertz is mostly used as a time domain point detection and capable of measuring both reflective and transmissive spectroscopy. In this thesis, only transmissive is used. Compared to MWIR, it is slow in point detection and throughput. In transmission mode, it shows promising ability to detect the effects of chemical additives if the thickness of the sample is known. The comparison of MWIR and THz specifications used for data/sensor fusion in this chapter can be seen in Table 2.

Table 2: MWIR vs THz

	MWIR	**THz**
Maturity	Mature	Under R&D
Domain	Frequency	Time
Spectroscopy	Reflective	Transmissive
Scan rate	380 Hz	Up to 160 Hz
Resolution	640 spatial by 308 spectral	4096 points/THz

3.1 Plastic Types

After the development of the THz-TDS based sorting system came to an end, high resolution spectrums of both THz and MWIR were gathered for different black plastic types. Different plastic types were purchased and cut into 12 x 12 inch samples. The available plastic samples are seen in the table below.

Table 3: Plastic types available for high resolution THz-TDS

Plastic	Color	Thickness (inches)
High-Density Polyethylene (PE)	Black, White	1/16, 1/8
Polycarbonate (PC)	Black, Clear	1/8
Acrylonitrile Butadiene Styrene (ABS)	Black, White	1/16, 1/8
High Impact Polystyrene (PS)	Black	1/8
Ultra-High Molecular Weight Polyethylene (UHMW)	Black, White	1/8
Polyoxymethylene (POM)	Black	1/8

High-resolution THz-TDS scans of all the plastics listed in Table 3 are taken at the CIARS THz lab at University of Waterloo. For gathering MWIR spectrum of black plastics, Specim kindly provided high-resolution scans of different types of black plastic with their latest MWIR camera, FX50. The provided MWIR spectrum of black plastic types were high-impact polystyrene (PS), acrylonitrile butadiene styrene (ABS) and high-density polyethylene (PE).

3.2 THz Spectrum

The plastic samples for the THz-TDS scanning were all cut into 12 x 12 inch sample sizes and had thicknesses of 1/16 and 1/8 inch. The samples were measured at 24°C with humidity of 47%. The optical pulse generated by the femtosecond laser had duration of 100 fs and central wavelength of 800 nm. The stage speed was 0.025 mm/s with scanning range of 14 mm. The THz spectroscopy of the black plastic samples were taken in the configuration seen in Figure 2. The average of the scanned samples can be seen in Figure 20 and 21 representing the time and frequency domain respectively.

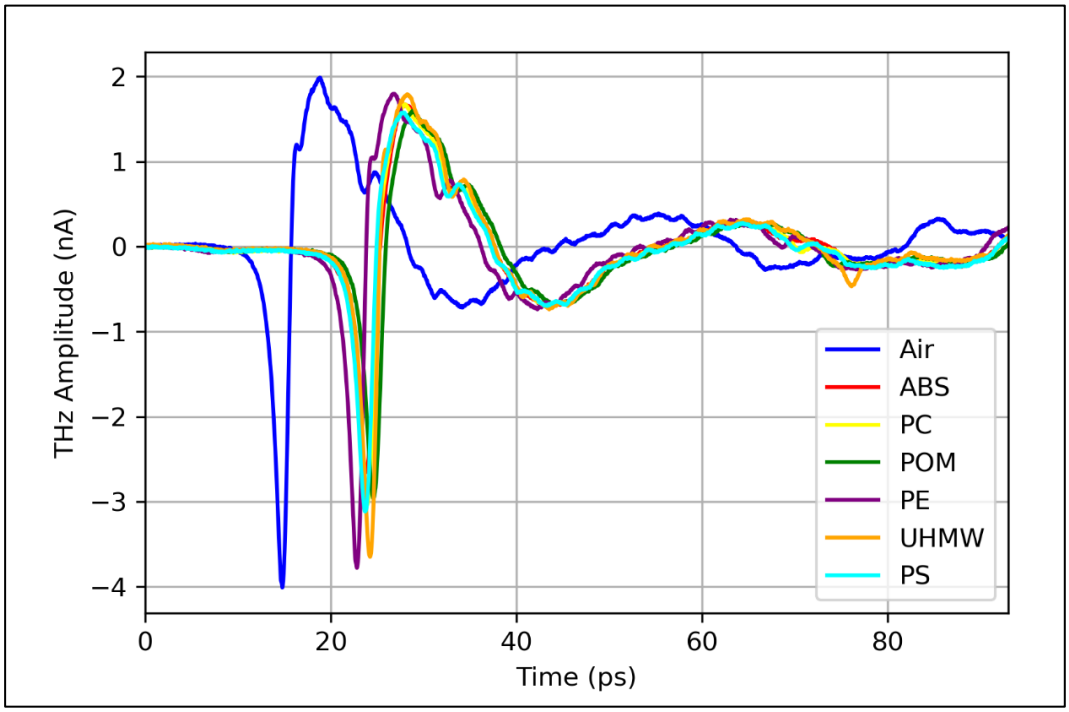

Figure 20: High resolution time-domain signal of black plastics

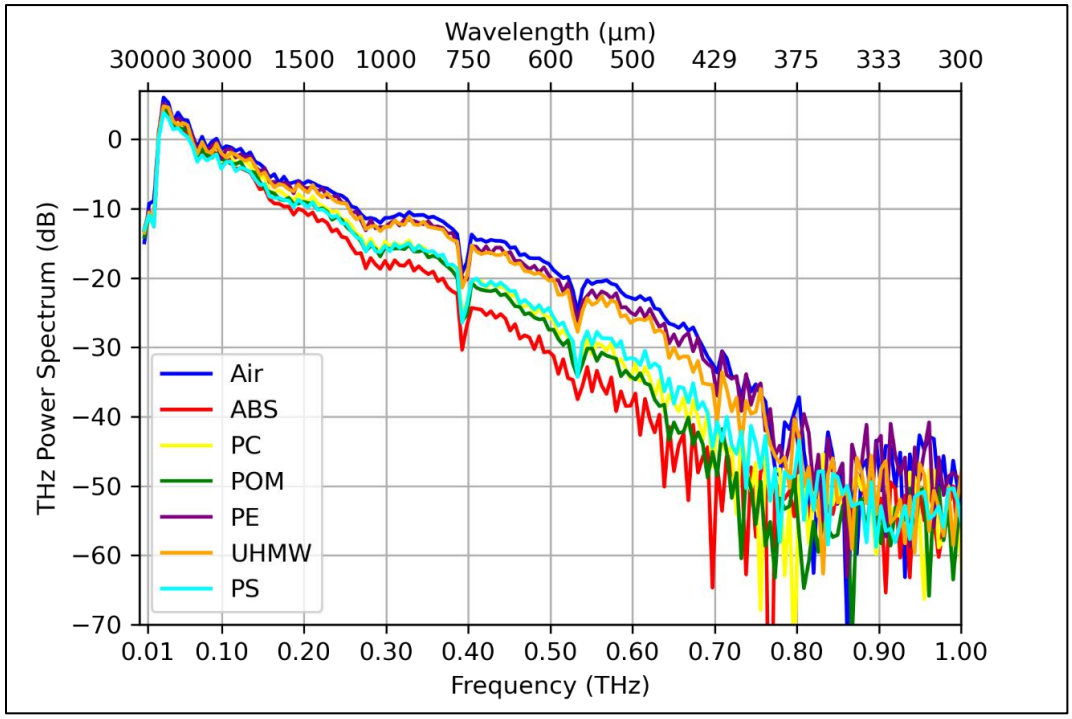

Figure 21: High resolution THz FFT of black plastics

We see that in the time-domain spectroscopy, all the black plastics have their own unique signatures. The time-domain signal of air is the THz signal of just air as its medium and the rest are the black plastic samples introduces in the air medium, hence the delay of the signals. From these measurements, the dielectric properties of the polymers can be calculated.

3.2.1 Complex Dielectric Properties of Black Plastics

One of the advantages of THz time-domain spectroscopy is that the dielectric properties of the measured sample can be extracted. From the measured THz-TDS signal, we want to extract the complex permittivity $\tilde{\varepsilon} = \varepsilon'(\omega) - j \cdot \varepsilon''(\omega)$ or equivalently, $\tilde{n} = n(\omega) - j \cdot k(\omega)$ which is the complex refractive index of the material. The complex frequency spectra of the reference (air) $\tilde{E}_{ref}$ and the sample (plastic) $\tilde{E}_{sam}$ are extracted from the FFT of the measured time-domain waveforms. The refractive index, n_s and its complex part, k_s of the measured plastic samples can be determined analytically from the ratio of $\tilde{E}_{ref}$ and $\tilde{E}_{sam}$ as follows [22]:

$$\frac{\tilde{E}_{sam}}{\tilde{E}_{ref}} = \rho(\omega) \cdot e^{-j\varphi(\omega)} \quad (1)$$

$$n_s(\omega) = \frac{c}{\omega d} \cdot \varphi(\omega) + 1 \quad (2)$$

$$k_s(\omega) = \frac{c}{\omega d} \cdot \ln\left(\frac{4n_s(\omega)}{\rho(\omega) \cdot (n_s(\omega) + 1))^2}\right) \quad (3)$$

Here, $\rho(\omega)$ denotes the magnitude, while $\varphi(\omega)$ denoted the phase of the two FFT signal ratio at the angular frequency, ω. The thickness of the sample is d and c is the speed of light in a vacuum. The absorption coefficient, α_s, can be calculated from the imaginary part of the refractive index, k_s, as,

$$\alpha_s(\omega) = \frac{2\omega k_s(\omega)}{c} \quad (4)$$

From the complex refractive index and the absorption coefficient, the real and imaginary part of the complex permittivity (dielectric constant) are calculated from the equations,

$$\varepsilon_s'(\omega) = n_s(\omega)^2 - \left(\frac{c\alpha_s(\omega)}{2\omega}\right)^2 \quad (5)$$

$$\varepsilon_s''(\omega) = 2\, n_s(\omega) k_s(\omega) \quad (6)$$

Finally, with the dielectric constant, the dielectric loss tangent can be determined as,

$$\tan\delta = \frac{\varepsilon_s''(\omega)}{\varepsilon_s'(\omega)} \quad (7)$$

The loss tangent denotes the dissipation of energy that goes into a material in a varying electric field. Using Equations, (1)-(7) the refractive index, absorption coefficient, and dielectric loss are calculated and can be seen in Figures 22 - 24.

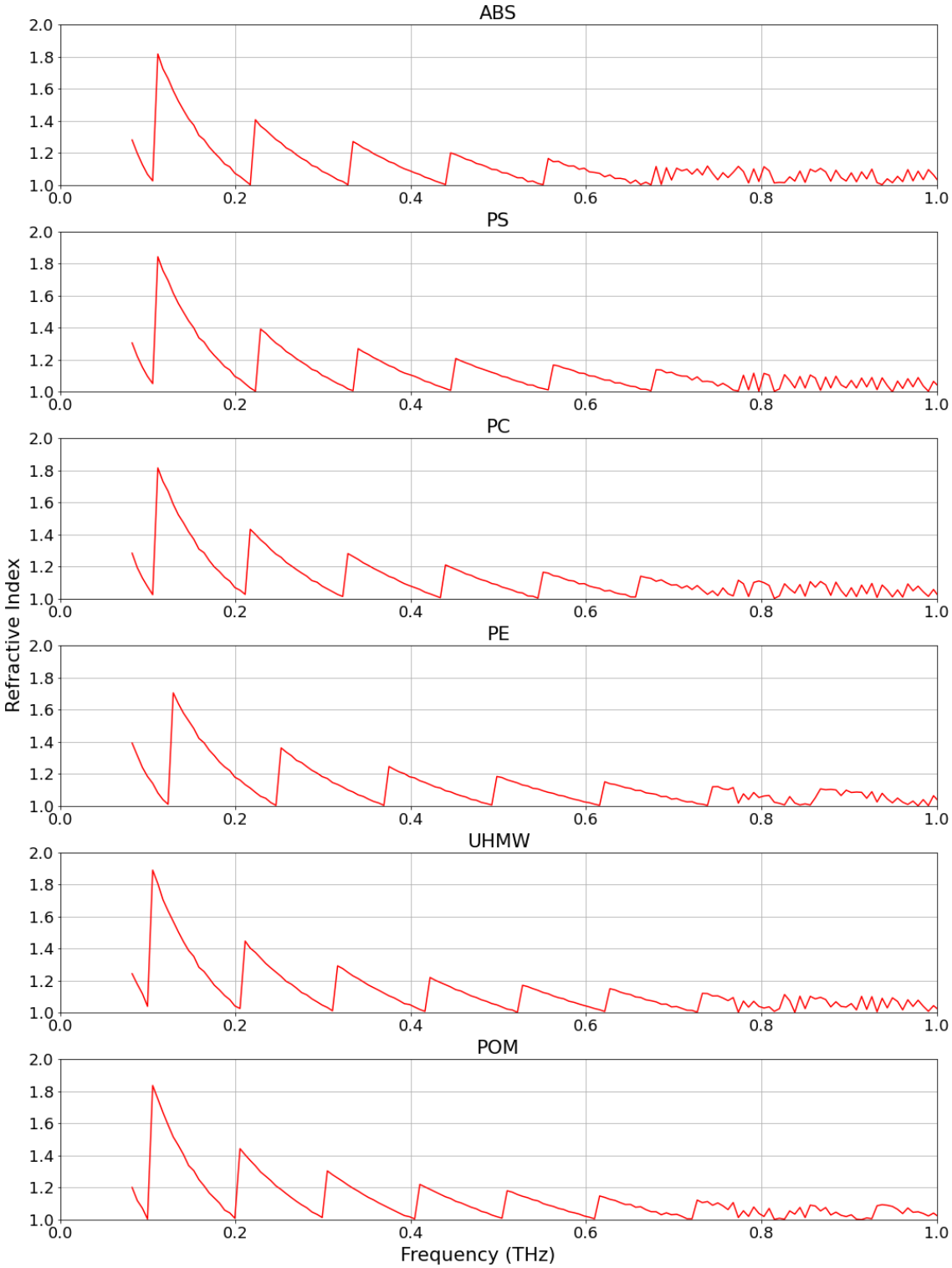

Figure 22: Calculated refractive index of black plastics

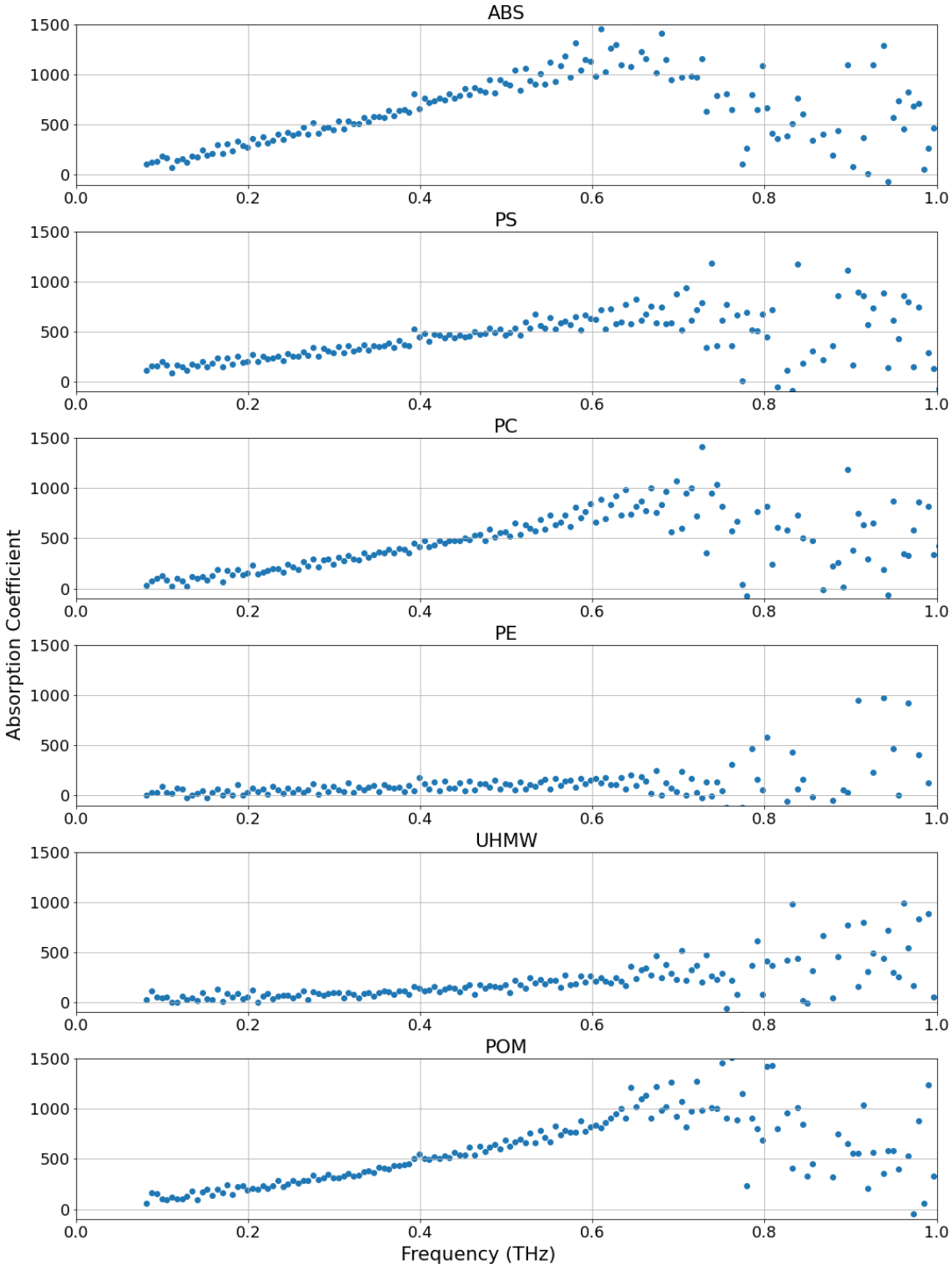

Figure 23: Calculated absorption coefficient of black plastics

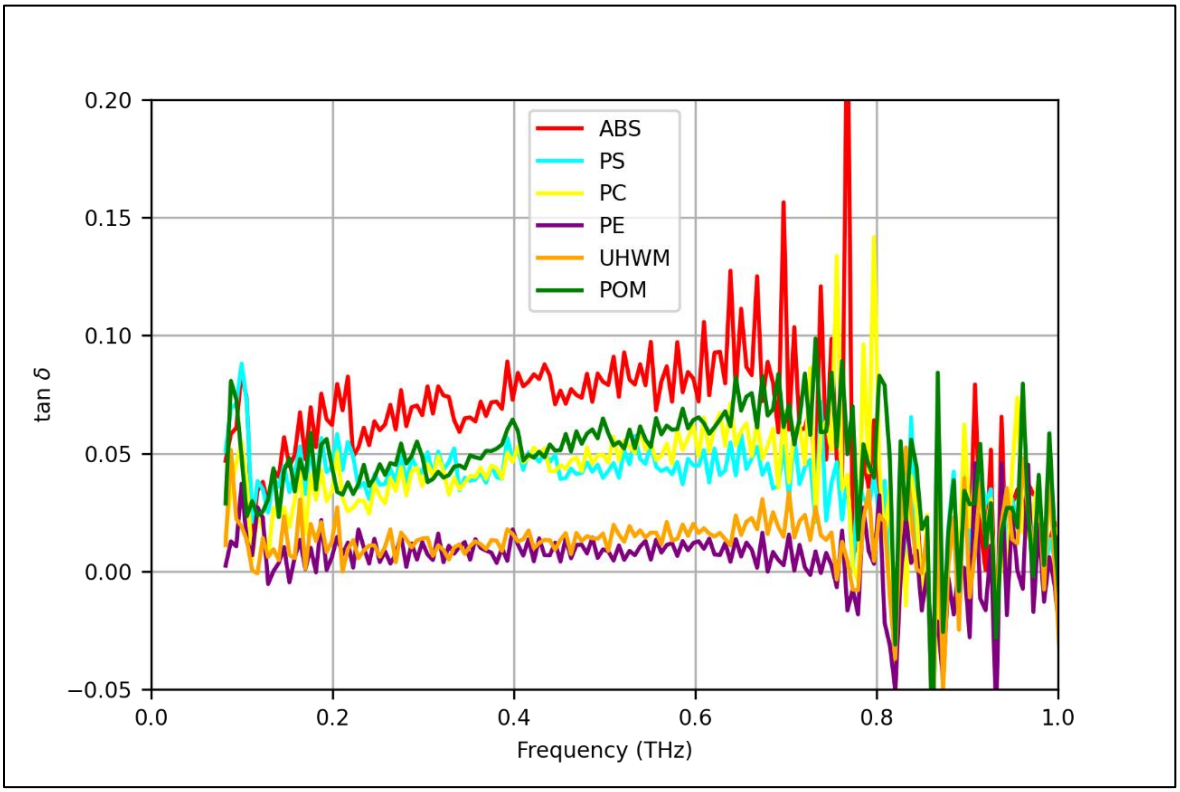

Figure 24: Calculated loss tangent of black plastics

By looking at the dielectric properties of the different black polymers, it is evident that there are frequencies that these plastics absorb differently than each other. We see the different variations at frequencies, 0.088 THz, 0.205 THz, 0.498THz, 0.527THz, 0.586 THz, 0.656 THz, 0.68THz, 0.727 THz, 0.75THz and 0.815THz. These identified frequencies can be visualized with principal component analysis (PCA).

3.2.2 PCA Visualization of THz bins

By focusing on the frequency identified after analyzing the dielectric properties, PCA is used to provide overview of the spectral data. The PCA of the THz spectrum with the focused frequencies can be seen in Figure 25. With three principal components, the THz spectral data seems to be easily distinguishable.

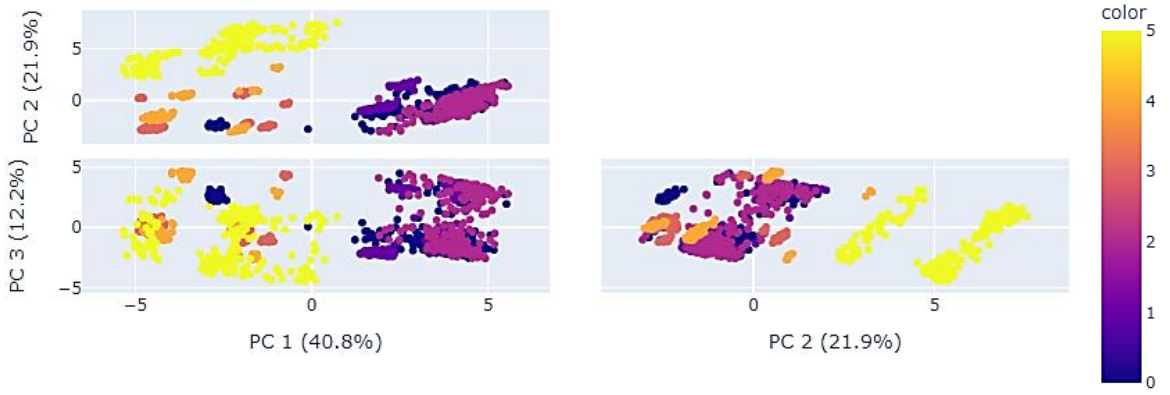

Figure 25: PCA on THz focused bins of black plastics (0:ABS, 1:PS, 2:PC, 3:PE, 4:UHMW, 5:POM)

3.2.3 Color Pigment on THz Spectra

The comparison of the THz spectra of plastic types with the same composition but different color pigments was performed. The analysis was performed on ABS, PC, PE and UHMW black plastics versus the same types but with different color pigment. All measured samples had the same thickness. The calculated refractive index, absorption coefficients and dielectric losses of the said plastics can be seen in Figures 26 - 28.

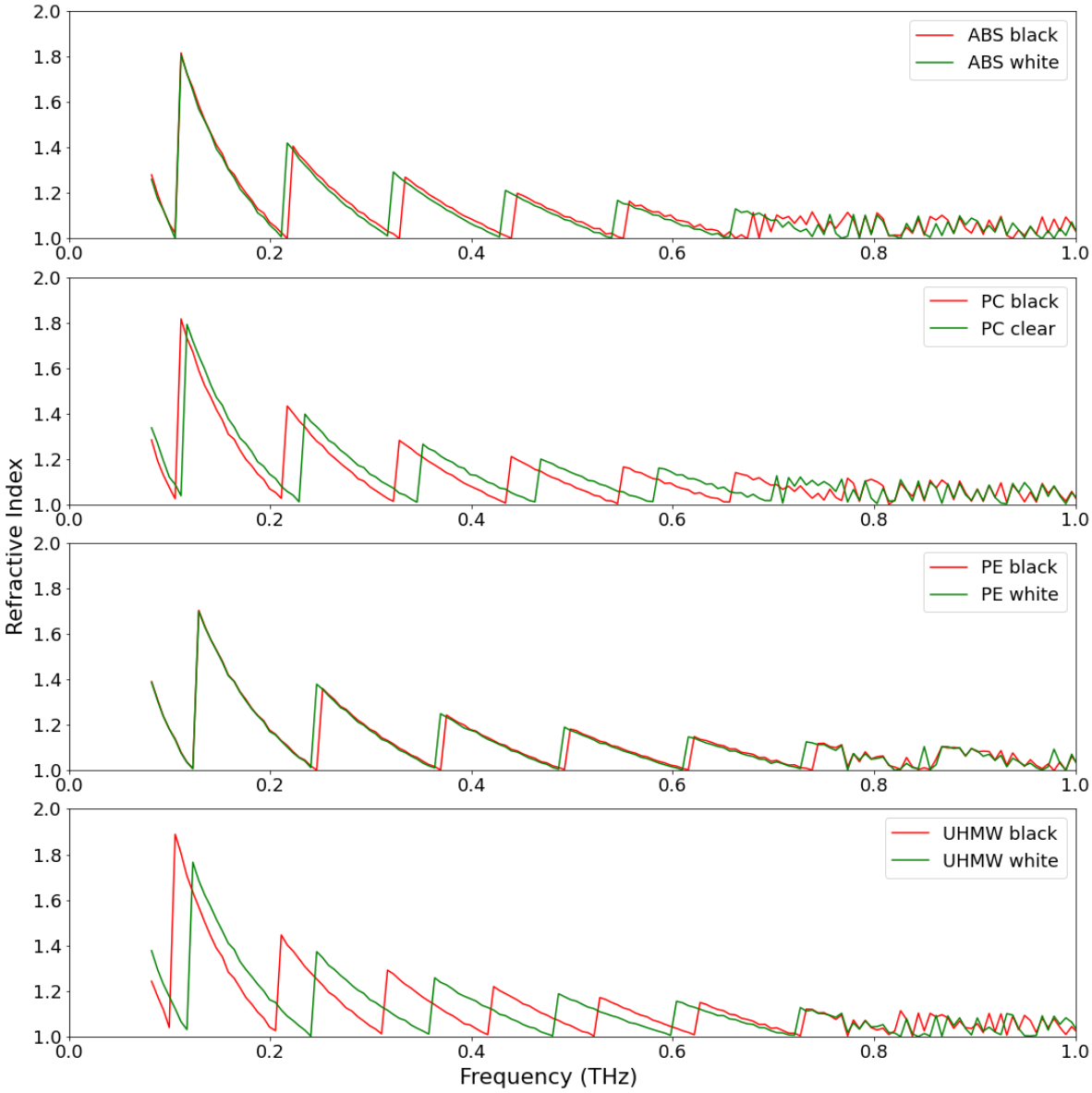

Figure 26 Refractive index of plastic types with different color pigment

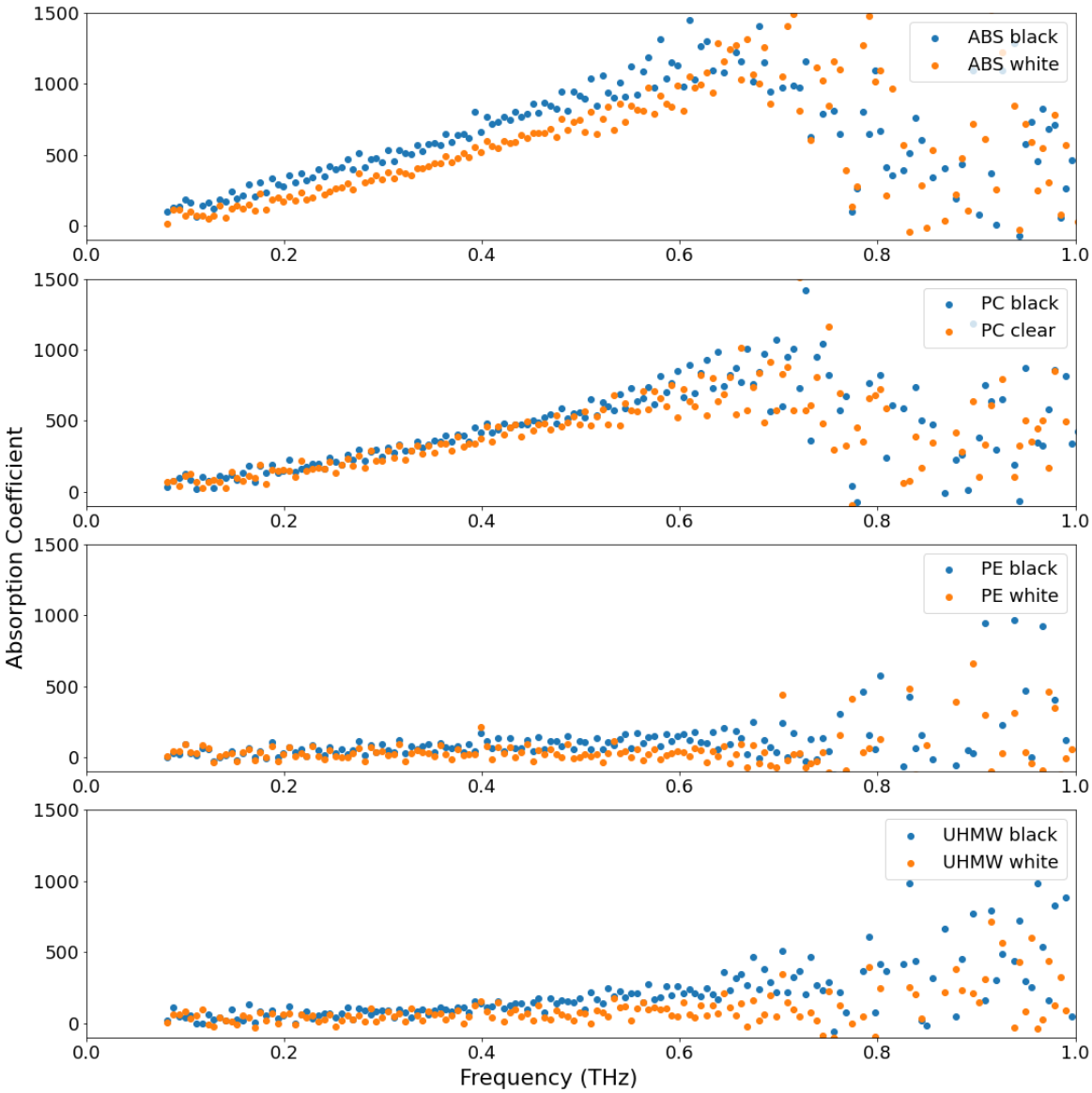

Figure 27: Absorption coefficient of plastic types with different color pigment

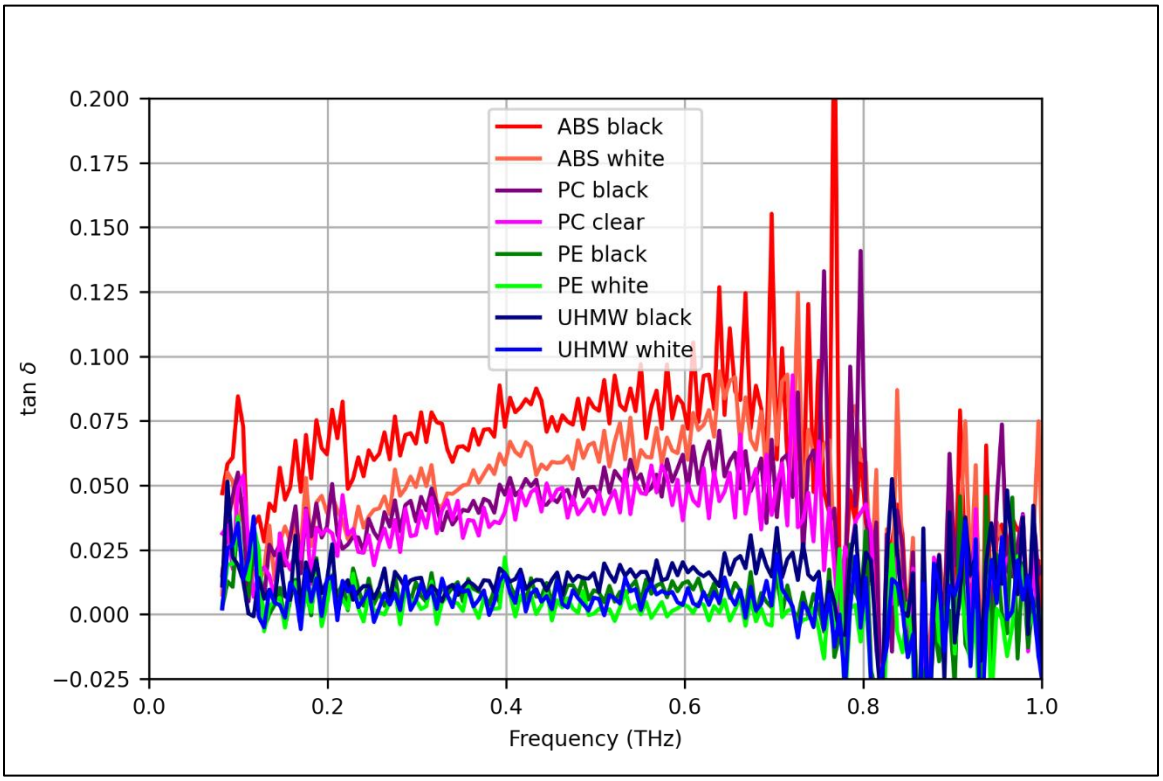

Figure 28: Loss tangent of plastics with different pigment

We see that ABS, PC, PE and UHWM ultimately have very similar dielectric properties as its colored counterparts. However, we see that color pigments have enough effect on THz radiation to have distinguishable features in the spectrum especially for ABS and PC.

3.3 MWIR Spectrum

The MWIR spectrum was kindly provided by Specim. Specim is a global leader in hyperspectral imaging, with many recycling plants using their cameras to sort different types of plastic [32]. The spectrum was captured using their FX50 camera. It is a high-speed line-scan camera that collect hyperspectral data in the medium wavelength infrared region from 2.7 to 5.3 μm with 8.44 nm spectral resolution (308 pixels). The spectral camera has spatial resolution of 640 pixels (more information can be seen in Appendix C). The captured spectrums are normalized by the white and dark references. The spectrum is normalized using the formula ((Value - Dark) / (White - Dark)). The average MWIR spectrum of black ABS, PS and PE are seen in Figure 29.

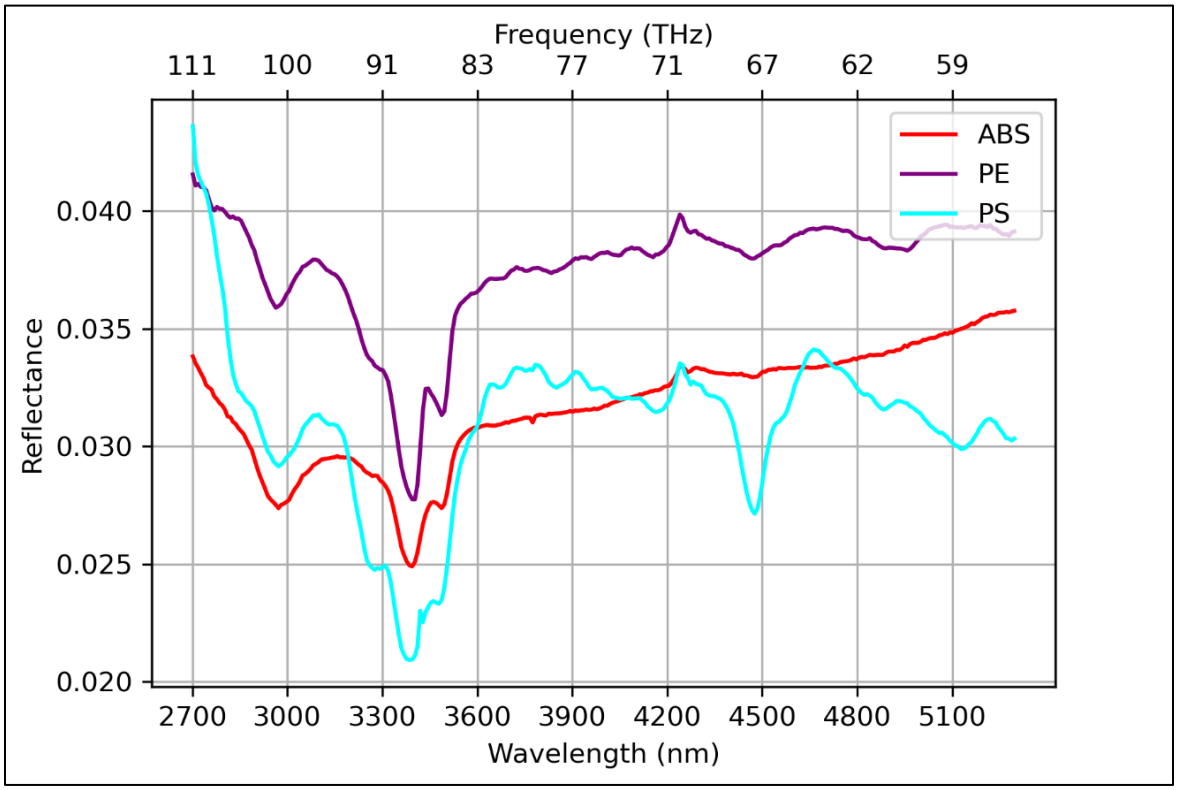

Figure 29: Average MWIR spectrum of black plastics

The raw MWIR spectra is very noisy for direct analysis. Therefore, data pre-processing is used to enhance the spectral features. Commonly in literature, pre-processing strategies such as scatter correction, spectral derivatives, and principal component analysis (PCA) are used [33]–[40].

3.3.1 Spectral Derivative

Savitzky-Goley smoothing and differentiation is used on the spectrum data to reduce noise and amplify small variations. The MWIR spectrum is applied the Savitzky-Goley filter and can be seen in Figure 30.

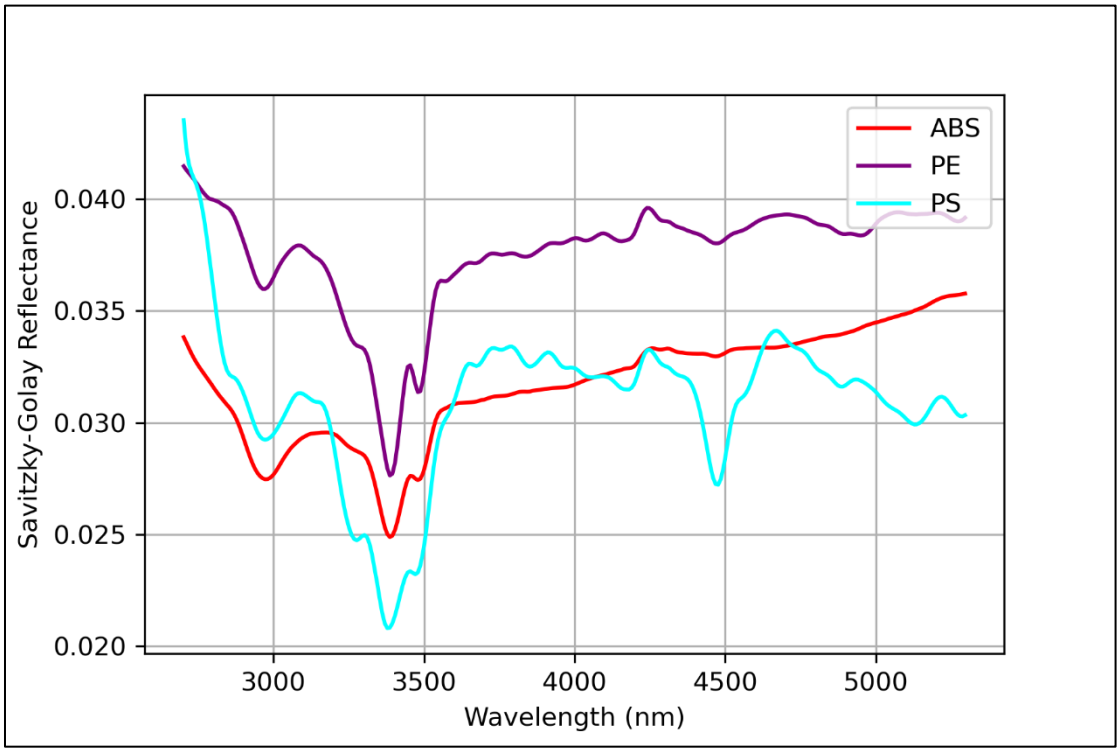

Figure 30: MWIR average spectra after Savitzky-Goley filter

3.3.2 Scatter Correction

Standard Normal Variate (SNV) is applied after the Savitzky-Goley filter. SNV transforms the measured spectrum into a signal with zero mean and uniform variance. By doing so, it removes all effects of unrelated chemical nature of the sample such as path length differences and particle size. The MWIR spectrum after SVN can be seen in Figure 31.

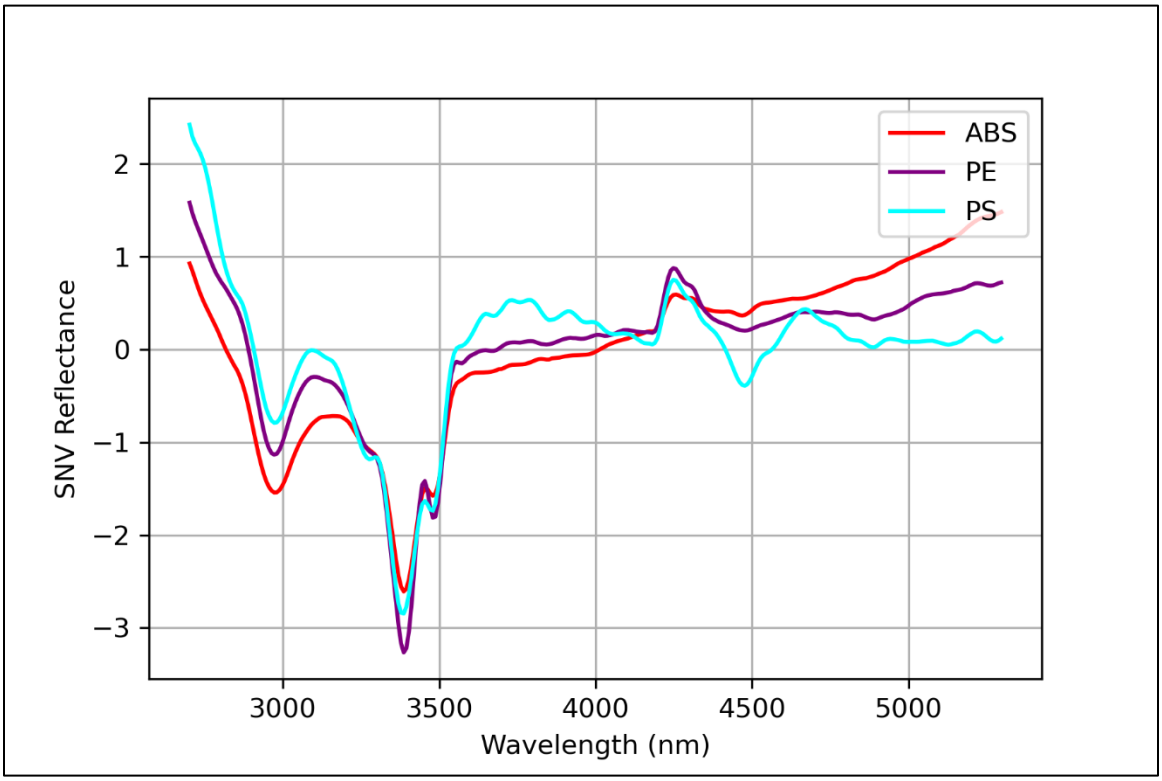

Figure 31: MWIR average spectra after scatter correction

We can see in Figure 31 that, that ABS, PE and PS have different absorptions at 2701nm, 2777nm, 3082nm, 3149 nm, 3394 nm, 3656nm, 3783nm, 3901nm, 4467nm, 5000 nm, and 5288 nm. These identified wavelengths can be visualized with principal component analysis.

3.3.3 PCA Visualization of MWIR bins

By focusing on the wavelength identified after scatter correction, PCA is used to provide overview of the spectral data. The PCA of the MWIR spectrum with the focused wavelengths can be seen in Figure 32. With three principal components, the MWIR spectral data is distinguishable.

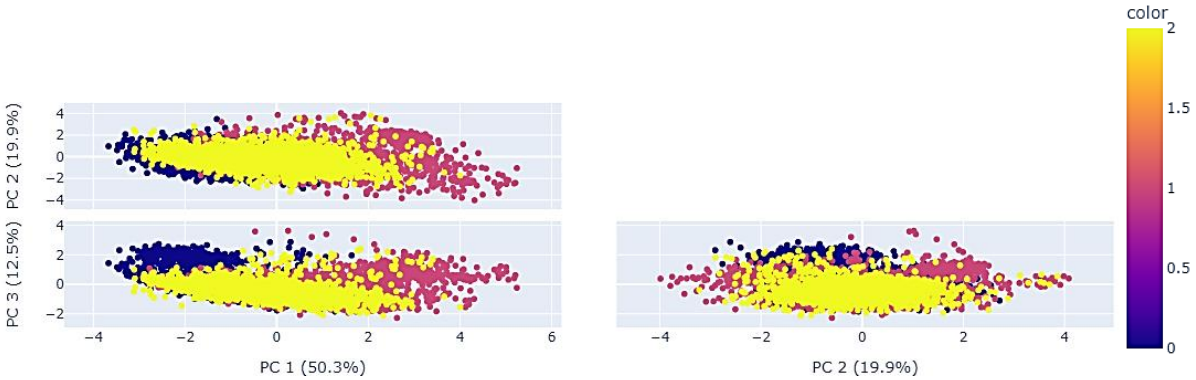

Figure 32: PCA of MWIR spectrum with focused bins (0: ABS, 1: PS, 2: PE)

3.4 THz and MWIR Data Fusion

Since we only have both THz and MWIR spectrums of black ABS, PS and PE, only these three plastics are used for data fusion. The THz FFT signals of the three black plastics are normalized with the air reference. Using the normalized THz spectrum, as well as the ten identified frequencies (THz bins), we can extract 20 features. Since the FFT gives both magnitude and phase at each THz bin. Secondly, the focused wavelengths (MWIR bins) identified from the MWIR spectrum analysis gives 11 features. Combining the focused THz and MWIR bins give total of 31 multispectral features what define the characteristics of the different black polymer types. The multispectral features are used train a classification model to simulate a sorting system. Three classification models are used to identify the different types of black plastic which are, Support Vector Machines (SVM), followed by a Fully Connected Neural Network (FCNN) and then a Convolutional Neural Network (CNN) which are commonly used in literature for spectral data. The architecture of the neural networks can be seen in Figure 33.

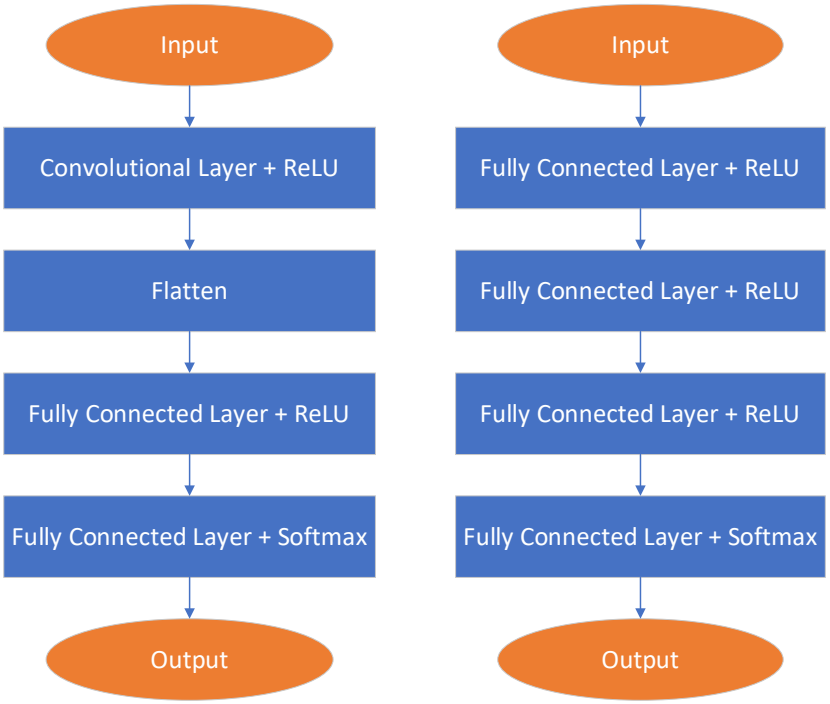

Figure 33: CNN Architecture (left) and FCNN Architecture (right)

3.4.1 Results

Using the combined spectral data of the black plastic types (ABS, PS and PE), the three models are trained and tested. The SVM classifier had accuracy of 96%. The FCNN and CNN both had accuracy of 100%. The confusion matrix of the classifiers are seen in the tables below.

Table 4: SVM confusion matrix

		Predicted		
		ABS	**PS**	**PE**
Actual	**ABS**	57	0	0
	PS	7	43	0
	PE	0	0	61

Table 5: FCNN and CNN confusion matrix

		Predicted		
		ABS	**PS**	**PE**
Actual	**ABS**	57	0	0
	PS	0	50	0
	PE	0	0	61

All the trained models identified the three black plastic types with very high accuracy. This validates that combining both THz and MWIR spectrums of different black plastic types provide enough information to sort them with high purity rate. As mentioned before MWIR is very sensitive to surface conditions, and THz is sensitive to thickness of the sample. By combining the data from both spectrums, we have proved that it can overcome these challenges as THz TDS in transmission mode is not as easily affected by surface conditions and MWIR is not affected by thickness of the sample. It is important to note that the used THz and MWIR data was very high resolution and captured in a controlled lab setting.

Chapter 4
Conclusion and Future Work

4.1 Conclusion

In this thesis, a novel approach to identifying e-waste black plastics with THz and MWIR technologies was studied. Identifying and sorting e-waste black plastics with just THz TDS was recognized with conditional requirements. The plastic size and thickness had to controlled due to the limitation of the scanning speed and the corresponding spectral information.

Secondly, the effective frequency bins that characterize e-waste black plastics was identified for both THz and MWIR regions. As well, successfully creating an effective classification algorithm to identify ABS, PS, and PE black plastics with very high accuracy using the combined multi-spectral bins. The classification models, SVM, FCNN, and CNN gave very promising results.

Additionally, THz technology is currently not mature enough to be applied in a real-time sorting application as discussed in Chapter 2. The scanning speed of THz technology needs to catch up with MWIR without loss of spectral information. However, thanks to the growing technologies of THz, MWIR and computing power, it is possible to sort different e-waste black plastics, especially ABS and PS, in real-time using the techniques discussed in this thesis. Real-time identification and sorting of different black plastics is essential for solving the crisis of e-waste and plastic pollution.

4.2 Future Work

There are several key issues that need to be addressed to implement a sorting system that is capable of segregating black plastics in real-time.

4.2.1 Improvements in Hardware

The next generation of sorting machines are most likely to utilize multiple (more than 2) sensor-based systems to obtain precise and optimum sorting of black plastics. In terms of the THz TDS set up used in this thesis, it is still early for it to be introduced to industrial recycling facilities, while MWIR cameras seem more suitable with its high-speed scanning and throughput. For further potential research, other low-cost alternatives can be investigated such as THz frequency multipliers and capacitive sensing.

THz frequency multipliers generate low THz frequencies by multiplying the frequency of the driver source in a nonlinear device to generate higher order harmonic frequencies. Schottky planer diodes can be used as they are simple and cost-effective in generating and detecting THz frequencies up to 2.5 THz [41]–[45]. Black plastics analyzed in this thesis were already distinguishable under 1 THz. This eliminates the need for expensive lasers and the complexity of fiber optic switches which were a major hurdle in developing an array of THz sensors in the THz based sorting system.

Capacitive sensing also has potential for future research. Capacitive sensors are able to measure the dielectric properties, mainly the electric permittivity of materials. Current studies have proven to be able to detect solid waste like paper and plastic[46], [47]. Addition of this sensor to the THz and MWIR combination could yield better real-time sorting and has potential for adoption due to its low cost.

4.2.2 Improvements in Plastic Identification

The spectral data used for identification were high resolution scans of clean samples collected in a lab setting in comparison to a plastic sample typically found in recycling facilities. More data collection and analysis of other plastic samples for both THz and MWIR need to be studied as data fusion was limited to ABS, PS, and PE in this thesis. Further studies could be on the low and high THz frequencies (up to 5 THz) on black polymer blends and aged black plastics.

Lastly, the trained classification model should be deployed with in the LabVIEW environment instead of running concurrently in a python script. This would be better suited for a time dependent system by reducing the TCP/ IP packet transmission and receival times between programs.

References

[1] "Plastic Pollution - Our World in Data".

[2] V. Sahajwalla and V. Gaikwad, "The present and future of e-waste plastics recycling," *Current Opinion in Green and Sustainable Chemistry*, vol. 13. Elsevier B.V., pp. 102–107, Oct. 01, 2018. doi: 10.1016/j.cogsc.2018.06.006.

[3] A. Turner, "Black plastics: Linear and circular economies, hazardous additives and marine pollution," *Environment International*, vol. 117. Elsevier Ltd, pp. 308–318, Aug. 01, 2018. doi: 10.1016/j.envint.2018.04.036.

[4] B. Tansel, "From electronic consumer products to e-wastes: Global outlook, waste quantities, recycling challenges," *Environment International*, vol. 98. Elsevier Ltd, pp. 35–45, Jan. 01, 2017. doi: 10.1016/j.envint.2016.10.002.

[5] J. Hopewell, R. Dvorak, and E. Kosior, "Plastics recycling: Challenges and opportunities," *Philosophical Transactions of the Royal Society B: Biological Sciences*, vol. 364, no. 1526. Royal Society, pp. 2115–2126, Jul. 27, 2009. doi: 10.1098/rstb.2008.0311.

[6] R. M. Bajracharya, A. C. Manalo, W. Karunasena, and K. tak Lau, "Characterisation of recycled mixed plastic solid wastes: Coupon and full-scale investigation," *Waste Management*, vol. 48, pp. 72–80, Feb. 2016, doi: 10.1016/j.wasman.2015.11.017.

[7] J. L. Lyche, C. Rosseland, G. Berge, and A. Polder, "Human health risk associated with brominated flame-retardants (BFRs)," *Environment International*, vol. 74, pp. 170–180, Jan. 2015, doi: 10.1016/j.envint.2014.09.006.

[8] R. A. Hites, J. A. Foran, S. J. Schwager, B. A. Knuth, M. C. Hamilton, and D. O. Carpenter, "Global Assessment of Polybrominated Diphenyl Ethers in Farmed and Wild Salmon," *Environmental Science & Technology*, vol. 38, no. 19, pp. 4945–4949, Oct. 2004, doi: 10.1021/es049548m.

[9] T. Hamers *et al.*, "In Vitro Profiling of the Endocrine-Disrupting Potency of Brominated Flame Retardants," *Toxicological Sciences*, vol. 92, no. 1, pp. 157–173, Jul. 2006, doi: 10.1093/toxsci/kfj187.

[10] I. A. Meerts *et al.*, “In vitro estrogenicity of polybrominated diphenyl ethers, hydroxylated PDBEs, and polybrominated bisphenol A compounds.,” *Environmental Health Perspectives*, vol. 109, no. 4, pp. 399–407, Apr. 2001, doi: 10.1289/ehp.01109399.

[11] K. Pivnenko, K. Granby, E. Eriksson, and T. F. Astrup, “Recycling of plastic waste: Screening for brominated flame retardants (BFRs),” *Waste Management*, vol. 69, pp. 101–109, Nov. 2017, doi: 10.1016/j.wasman.2017.08.038.

[12] C. Pharino, *Challenges for Sustainable Solid Waste Management*. Singapore: Springer Singapore, 2017. doi: 10.1007/978-981-10-4631-5.

[13] J. Gasde, J. Woidasky, J. Moesslein, and C. Lang-Koetz, “Plastics Recycling with Tracer-Based-Sorting: Challenges of a Potential Radical Technology,” *Sustainability*, vol. 13, no. 1, p. 258, Dec. 2020, doi: 10.3390/su13010258.

[14] A. Tehrani and H. Karbasi, “A novel integration of hyper-spectral imaging and neural networks to process waste electrical and electronic plastics,” 2017.

[15] R. M. Groves, B. Pradarutti, E. Kouloumpi, W. Osten, and G. Notni, “2D and 3D non-destructive evaluation of a wooden panel painting using shearography and terahertz imaging,” *NDT & E International*, vol. 42, no. 6, pp. 543–549, Sep. 2009, doi: 10.1016/j.ndteint.2009.04.002.

[16] D. Markl, M. T. Ruggiero, and J. A. Zeitler, “Pharmaceutical applications of terahertz spectroscopy and imaging Solid-state anharmonic properties View project Terahertz Spectroscopy View project.” [Online]. Available: https://www.researchgate.net/publication/309251209

[17] P. F. Taday, “Applications of terahertz spectroscopy to pharmaceutical sciences,” *Philosophical Transactions of the Royal Society of London. Series A: Mathematical, Physical and Engineering Sciences*, vol. 362, no. 1815, pp. 351–364, Feb. 2004, doi: 10.1098/rsta.2003.1321.

[18] P. C. Ashworth *et al.*, “Terahertz pulsed spectroscopy of freshly excised human breast cancer,” *Optics Express*, vol. 17, no. 15, p. 12444, Jul. 2009, doi: 10.1364/oe.17.012444.

[19] V. L. Vaks, A. v. Illyuk, A. N. Panin, S. I. Pripolsin, S. S. Nabiev, and D. B. Stavrovskii, “Subterahertz and mid IR spectroscopy of explosive substances,” in *Proceedings - TERA-MIR*

2009, NATO Advanced Research Workshop Terahertz and Mid Infrared Radiation: Basic Research and Practical Applications, 2009, pp. 91–92. doi: 10.1109/TERAMIR.2009.5379612.

[20] H. Hoshina, Y. Sasaki, A. Hayashi, C. Otani, and K. Kawase, "Noninvasive Mail Inspection System with Terahertz Radiation," *Appl. Spectrosc.*, vol. 63, no. 1, pp. 81–86, Jan. 2009, [Online]. Available: http://opg.optica.org/as/abstract.cfm?URI=as-63-1-81

[21] S. Wietzke *et al.*, "Terahertz spectroscopy - A powerful tool for the characterization of plastic materials," 2010. doi: 10.1109/ICSD.2010.5567915.

[22] Y.-S. Jin, G.-J. Kim, and S.-G. Jeon, "Terahertz Dielectric Properties of Polymers," 2006.

[23] Theophanides Theophile, *Infrared Spectroscopy - Materials Science, Engineering and Technology*. InTech, 2012. doi: 10.5772/2055.

[24] M. Chatzidakis and G. A. Botton, "Towards calibration-invariant spectroscopy using deep learning," *Scientific Reports*, vol. 9, no. 1, Dec. 2019, doi: 10.1038/s41598-019-38482-1.

[25] A. C. Karaca, A. Erturk, M. K. Gullu, M. M. Elmas, and S. Erturk, "Automatic waste sorting using shortwave infrared hyperspectral imaging system," in *Workshop on Hyperspectral Image and Signal Processing, Evolution in Remote Sensing*, Jun. 2013, vol. 2013-June. doi: 10.1109/WHISPERS.2013.8080744.

[26] G. Bonifazi, G. Capobianco, and S. Serranti, "A hierarchical classification approach for recognition of low-density (LDPE) and high-density polyethylene (HDPE) in mixed plastic waste based on short-wave infrared (SWIR) hyperspectral imaging," *Spectrochimica Acta - Part A: Molecular and Biomolecular Spectroscopy*, vol. 198, pp. 115–122, Jun. 2018, doi: 10.1016/j.saa.2018.03.006.

[27] G. Bonifazi, F. di Maio, F. Potenza, and S. Serranti, "FT-IR spectroscopy and hyperspectral imaging applied to post-consumer plastic packaging characterization and sorting," in *Proceedings of IEEE Sensors*, Dec. 2014, vol. 2014-December, no. December, pp. 633–636. doi: 10.1109/ICSENS.2014.6985078.

[28] G. Bonifazi, L. Fiore, R. Gasbarrone, P. Hennebert, and S. Serranti, "Detection of Brominated Plastics from E-Waste by Short-Wave Infrared Spectroscopy," 2021, doi: 10.3390/recycling6030054.

[29] J. Neu and C. A. Schmuttenmaer, “Tutorial: An introduction to terahertz time domain spectroscopy (THz-TDS),” *Journal of Applied Physics*, vol. 124, no. 23, Dec. 2018, doi: 10.1063/1.5047659.

[30] “OPTICAL MEMS SWITCHES SC 1xN,” *https://www.sercalo.com/products/mems-switches-products/sc*.

[31] D Saeedkia, *Handbook of Terahertz Technology for Imaging, Sensing and Communications*, 1st ed. Oxford (GB): Woodhead publ., 2013.

[32] Specim, “Hyperspectral imaging cameras and systems,” *https://www.specim.fi/*, Jan. 02, 2022.

[33] W. Camacho and S. Karlsson, “Quantification of Antioxidants in Polyethylene by Near Infrared (NIR) Analysis and Partial Least Squares (PLS) Regression,” *International Journal of Polymer Analysis and Characterization*, vol. 7, no. 1–2, pp. 41–51, Jan. 2002, doi: 10.1080/10236660214597.

[34] S. Serranti, A. Gargiulo, and G. Bonifazi, “Hyperspectral Imaging for Process and Quality Control in Recycling Plants of Polyolefin Flakes,” *Journal of Near Infrared Spectroscopy*, vol. 20, no. 5, pp. 573–581, Oct. 2012, doi: 10.1255/jnirs.1016.

[35] R. Calvini, A. Ulrici, and J. M. Amigo, “Practical comparison of sparse methods for classification of Arabica and Robusta coffee species using near infrared hyperspectral imaging,” *Chemometrics and Intelligent Laboratory Systems*, vol. 146, pp. 503–511, Aug. 2015, doi: 10.1016/j.chemolab.2015.07.010.

[36] M. Blanco, M. Alcalá, J. M. González, and E. Torras, “A process analytical technology approach based on near infrared spectroscopy: Tablet hardness, content uniformity, and dissolution test measurements of intact tablets,” *Journal of Pharmaceutical Sciences*, vol. 95, no. 10, pp. 2137–2144, Oct. 2006, doi: 10.1002/jps.20653.

[37] Y.-Z. Feng and D.-W. Sun, “Near-infrared hyperspectral imaging in tandem with partial least squares regression and genetic algorithm for non-destructive determination and visualization of Pseudomonas loads in chicken fillets,” *Talanta*, vol. 109, pp. 74–83, May 2013, doi: 10.1016/j.talanta.2013.01.057.

[38] I. González-Martín, C. González-Pérez, J. Hernández-Méndez, and N. Alvarez-García, “Determination of fatty acids in the subcutaneous fat of Iberian breed swine by near infrared

spectroscopy (NIRS) with a fibre-optic probe," *Meat Science*, vol. 65, no. 2, pp. 713–719, Oct. 2003, doi: 10.1016/S0309-1740(02)00273-5.

[39] Åsmund Rinnan, F. van den Berg, and S. B. Engelsen, "Review of the most common pre-processing techniques for near-infrared spectra," *TrAC Trends in Analytical Chemistry*, vol. 28, no. 10, pp. 1201–1222, Nov. 2009, doi: 10.1016/j.trac.2009.07.007.

[40] M. Vidal and J. M. Amigo, "Pre-processing of hyperspectral images. Essential steps before image analysis," *Chemometrics and Intelligent Laboratory Systems*, vol. 117, pp. 138–148, Aug. 2012, doi: 10.1016/j.chemolab.2012.05.009.

[41] D. Saeedkia and S. Safavi-Naeini, "Terahertz photonics: Optoelectronic techniques for generation and detection of Terahertz waves," *Journal of Lightwave Technology*, vol. 26, no. 15, pp. 2409–2423, 2008, doi: 10.1109/JLT.2008.927614.

[42] A. Maestrini, J. Ward, G. Chattopadhyay, E. Schlecht, and I. Mehdi, "Terahertz sources based on frequency multiplication and their applications," *Frequenz*, vol. 62, no. 5–6, pp. 118–122, 2008, doi: 10.1515/FREQ.2008.62.5-6.118.

[43] A. Maestrini *et al.*, "Multiplicateurs de fréquences et mélangeurs THz utilisant des diodes Schottky," *Comptes Rendus Physique*, vol. 11, no. 7–8. pp. 480–495, Aug. 2010. doi: 10.1016/j.crhy.2010.05.002.

[44] M. Schiselski *et al.*, "A planar Schottky diode based integrated THz detector for fast electron pulse diagnostics," in *IEEE MTT-S International Microwave Symposium Digest*, Aug. 2016, vol. 2016-August. doi: 10.1109/MWSYM.2016.7540173.

[45] J. Grajal and B. Leone, "Analytical modelling of THz frequency multipliers and mixers based on Schottky diodes," 2005. [Online]. Available: https://www.researchgate.net/publication/253431322

[46] C. Zet, C. Fosalau, and A. Hariton, "Study on the possibilities of detecting recyclable waste using the dielectric properties of materials," in *SIELMEN 2021 - Proceedings of the 11th International Conference on Electromechanical and Energy Systems*, 2021, pp. 444–447. doi: 10.1109/SIELMEN53755.2021.9600360.

[47] I. Kabir Ahmad, M. Mukhlisin, and H. Basri, "Application of Capacitance Proximity Sensor for the Identification of Paper and Plastic from Recycling Materials," *Research Journal of*

Applied Sciences, Engineering and Technology, vol. 12, no. 12, pp. 1221–1228, Jun. 2016, doi: 10.19026/rjaset.12.2880.

Appendices

Appendix A

Rigel 1550 Terahertz Spectrometer

Rigel 1550 Terahertz Spectrometer

Key Features

- Modular, fast, reconfigurable, compact, and portable
- Fiber coupled and movable transmitter and receiver heads
- High speed scan
- Built-in data acquisition, data processing, and data display software
- Adjustable scan speed, scan range, and averaging time
- Transmission, reflection, and attenuated total reflection measurement modules
- Turn-key and easy to operate
- Nitrogen purge option
- Intuitive user interface

Product Overview

The TeTechS Rigel™ 1550 is a portable, modular, fast, reconfigurable, and compact terahertz time-domain spectrometer system for analysis of solids, liquids, powders, and gases. The fiber coupled movable transmitter and receiver heads can be mounted around the sample under test, for the cases where bringing the sample/process under test inside the spectrometer head is not feasible. The distance between the transmitter and receiver heads can be adjusted to create working space needed for different measurement settings.

Rigel 1550 provides considerably higher performance and flexibility than the state of the art today in fiber coupled 1550 terahertz time-domain systems, allowing better discrimination, less complex signal analysis, and enabling applications which cannot be robustly achieved with previous terahertz spectrometry technology.

The TeTechS Rigel 1550 is an innovative and reliable turnkey system with a built-in 1550 nm femto-second fiber laser, a fiber laser beam distribution chassis with fast and slow scan modules, and built-in lock-in and low-noise amplifiers, with a controlling and operation software.

The system is permanently aligned to provide a collimated terahertz beam between the transmitter and the receiver heads. The user has access to the collimated terahertz beam inside the spectrometer head where the inter-changeable and easy to use transmission, reflection, and attenuated total reflection (ATR) measurement modules can be placed.

Product Specifications

Scaning Mode	Slow and Fast Scan
Slow Scan Range	up to 1.3 ns
Fast Scan Range	up to 65 ps
Slow Scan Speed	10 µm/s to 0.5 mm/s
Fast Scan Rate	up to 20 waveforms/s
Terahertz Bandwidth	>1 THz
Spectrum Dynamic Range	> 55 dB slow scan; > 40 dB fast scan
Laser Wavelength	1559 nm
Size (W X L X H)	60 cm X 60 cm X 105 cm
Weight	250 lbs

Address: 295 Hagey Blvd, 1st Floor, Waterloo, Ontario N2L 6R5, Canada
Toll Free (Canada & USA): +1 855.574.1764
Phone: +1 519.584.0791
Fax: +1 519.513.2421
Email: info@tetechs.com
Web: www.tetechs.com

TeTechS Inc.

Appendix B

Sercalo Fiber Optic SC1x4 switch

FIBER OPTIC 1xN SWITCH

coaxial design

OVERVIEW

sercalo's fiber optic 1xN switches are bidirectional opto-mechanical switches based on a coaxial design where a single MEMS mirror redirects light from a common fiber to one of N ports. The MEMS technology results in low insertion loss and low crosstalk between channels while keeping a constant switching performance over life.

The switch is available in several different variants to simplify integration in existing systems and reduce development cost. The miniature packages withstands rugged environments and is well suited for direct mounting on printed circuit boards.

The hermetically sealed MEMS and the laser welded fiber collimator guarantee broad temperature range and superior long-term stability. No epoxy is present in the optical path.

The component is compliant to Telcordia 1221 reliability standards and RoHS requirements 2015/863/EU.

FEATURES

- Low insertion loss
- Reliable
- Up to 1x36 optical ports
- UART, I²C/SMBus and parallel interface
- Ethernet interface available on request
- RoHS compliant

APPLICATIONS

- Optical network switching
- Instrumentation
- Test and measurement

Contact:
Sercalo Microtechnology Ltd.
Landstrasse 151
9494 Schaan - Principality of Liechtenstein
Tel. +423 237 57 97 Fax. +423 237 57 48
www.sercalo.com e-mail: info@sercalo.com

ORDERING INFORMATION

-	SC	1x4	-	9	R	-	05	FP

Package type
none = standard package
bc = bare component
m = miniature
r = industry compatible

Switch type
SC

Ports
1x4
1x8
1x12
1x16
1x24
1x32
up to
1x36

Fiber type
9 = SMF28ULTRA
9PM = PM15-U40A
(Corning Panda fiber)
7 = SM980 for 1050nm
4 = SM600 for 630nm
Other fiber types and wavelengths upon request

Fiber sleeve type
B = 250µm bare fibers
R = 8-fibers or 12-fibers ribbon
N = 900 µm sleeve (on rSC only)

Pigtail length
Expressed in decimeters
e.g.:
05 = 50 cm
10 = 100 cm

Connectors type
none = no connectors
FP = FC-PC
FA = FC-APC narrow key
LP = LC-PC
SA = SC-APC
SP = SC-PC

sercalo

sercalo's COAXIAL TYPE 1xN switch is non-latching: at power-off it breaks the optical connection and routing of the common port is not defined. The component is bidirectional, the common port can be used as input or output. The **PM Panda version** is offered up to 1x4 ports.

The switch is available in four different variants:
SC: standard size – ribbon fibers
mSC: miniature size – small driver board: 7x40 mm
rSC: compatible with industry pinout
bcSC: bare optical component

TECHNICAL SPECIFICATIONS

		Unit	Min	Typ	Max
Optical Specifications					
Wavelength range		nm	1250		1670
Insertion loss up to 1x4[1]		dB		0.4	1.0
Insertion loss up to 1x16[1]		dB		0.8	1.2
Insertion loss up to 1x24[1]		dB		1.0	1.5
Insertion loss up to 1x36[1]		dB		1.2	2.0
Crosstalk		dB	50	60	
Polarization dependent loss		dB			0.1
Return loss		dB	50	55	
Wavelength dependent loss (one band)		dB			0.2
Wavelength dependent loss (1250–1670 nm)		dB		0.5	1.0
Temperature dependent loss		dB			0.2
Maximum optical power level[2]		mW			500
Switching time		ms		5	10
Cycle rate		Hz		10	50
Repeatability[3]		dB			0.01
Durability		cycles		No wear out	
Optical Specifications (PM fiber - up to 1x4)					
Polarization extinction ratio		dB	20		
Electrical Specifications (SC, mSC, rSC)					
Supply voltage		V	4.75	5	5.25
Power consumption, normal mode		mW			150
Power consumption, standby		mW		40	
UART speed		baud	9600		115200
SMBus/I²C bus speed		kbps			400
Input logic level low		V		0	0.6
Input logic level high		V	2.4	5	
Output logic level low		V		0	0.6
Output logic level high		V	2.6	3.3	
Reset inactive voltage[4]		V	2.4	5	
Reset active voltage		V		0	0.9
Reset pulse duration		µs	15		
Electrical Specifications (bcSC)					
Driving voltage		V	0		
Driving voltage damage threshold		V			45
Electrostatic discharge tolerance[5]		V			50
Package					
Operating temperature		°C	-10		70
Storage temperature		°C	-40		85
Operation humidity (non condensing)		% r.h.	0		95
Pigtail length		cm	50		100
Dimensions	SC	mm		40 x 21 x 7	
	mSC	mm		40 x 7 x 7.5	
	rSC	mm		68 x 30 x 9	
	bcSC	mm		∅6 x 35	
ROHS Compliance				2015/863/EU (no exceptions)	

[1] Values at 25 °C at 1550 nm, without connectors. For operation over several bands 1250 to 1670 add 0.5 dB. [2] It is recommended to turn off the laser during switch transients when switching optical power above 100 mW. [3]For constant temperature and polarization. [4]Through onboard pull-up resistor. [5] The bare optical component is not protected against ESD.

FUNCTIONAL BLOC DIAGRAM

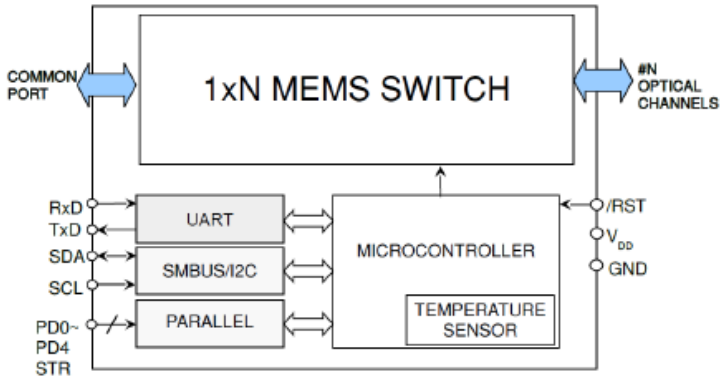

SC STANDARD SIZE – DIMENSIONS AND PINOUT

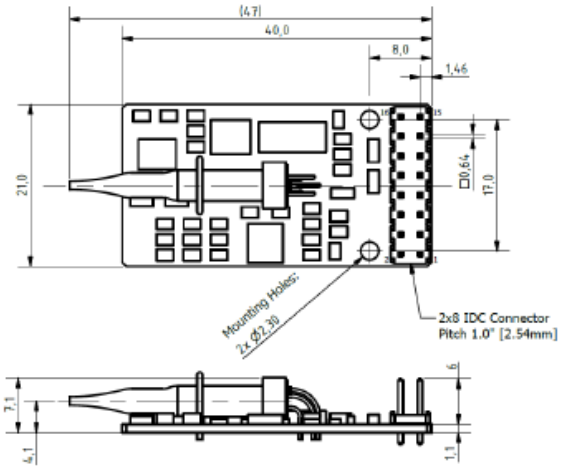

Pin number	*Description*
1	Parallel PD3
2	Parallel PD4
3	Parallel PD1
4	Parallel PD2
5	Parallel STROBE/ENABLE
6	Parallel PD0
7	Ground (GND)
8	Supply voltage (V_{DD})
9	Reserved
10	UART TX
11	Reserved
12	UART RX
13	System reset (RST)
14	SMBus/I²C SDA
15	SMBus/I²C SCL
16	Ground (GND)

mSC MINIATURE – DIMENSIONS AND PINOUT

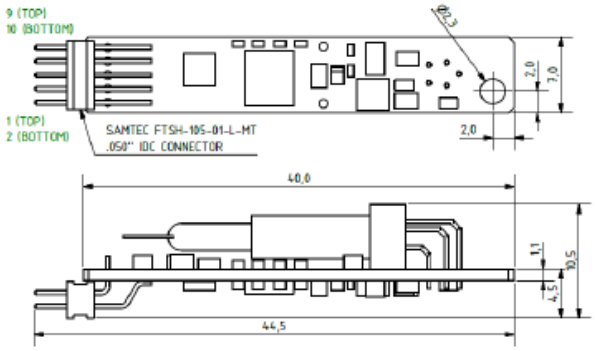

Pin number	*Description*
1	I/F mode
2	Supply voltage (V_{DD})
3	System reset (RST)
4	Ground (GND)
5	SMBus/I²C A0
6	SMBus/I²C A2 / UART RX
7	SMBus/I²C A1 / UART TX
8	SMBus/I²C SCL
9	SMBus/I²C A3
10	SMBus/I²C SDA

rSC INDUSTRY COMPATIBLE – DIMENSIONS AND PINOUT

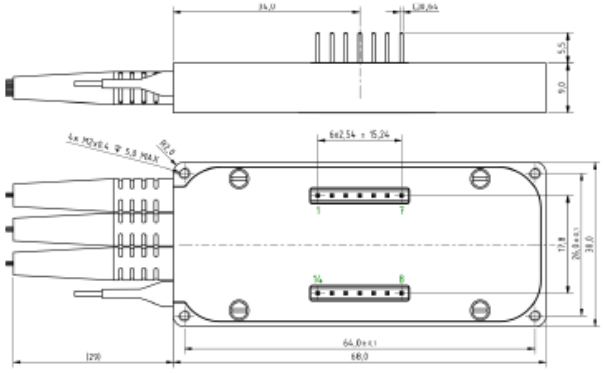

Pin number	*Description*
1	I/F mode 1
2	Supply voltage (V_{DD})
3	Parallel strobe
4	Ground (GND)
5	Parallel D0 / SMBus/I²C A0
6	SMBus/I²C SDA / UART TX
7	SMBus/I²C SCL / UART RX
8	I/F mode 0
9	Parallel D2 / SMBus/I²C A2
10	Done
11	Ground (GND)
12	Parallel D1 / SMBus/I²C A1
13	Parallel D3 / SMBus/I²C A3
14	System reset (RST)

bcSC BARE OPTICAL COMPONENT – DIMENSIONS AND PINOUT

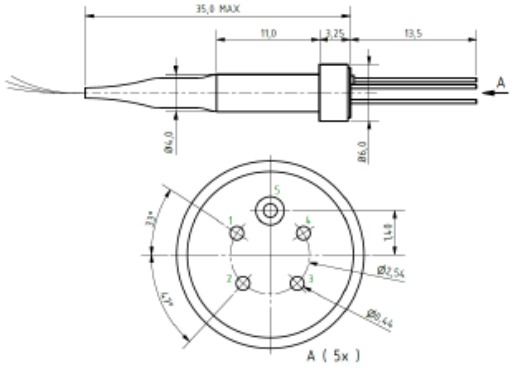

Pin number	*Description*
1	Axis X-
2	Axis Y-
3	Axis X+
4	Axis Y+
5	Common

INSERTION LOSS vs. TEMPERATURE (SC 1x8)

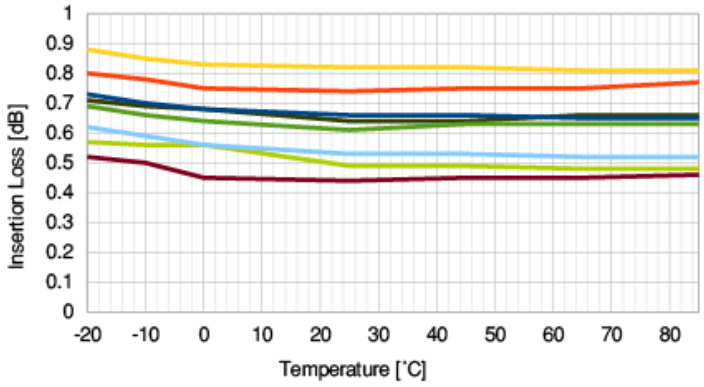

WAVELENGTH DEPENDENT LOSS (SC 1x4)

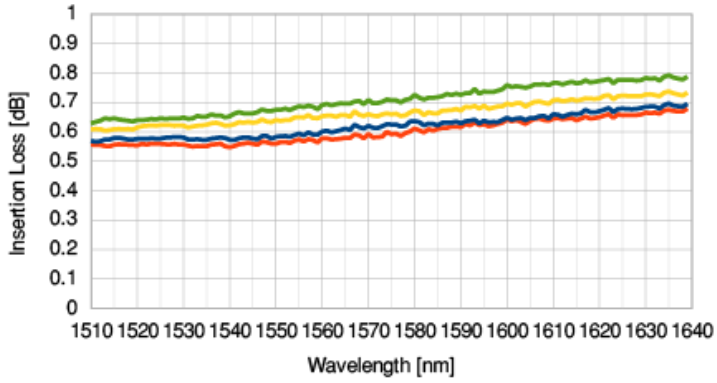

OPTICAL RESPONSE TIME

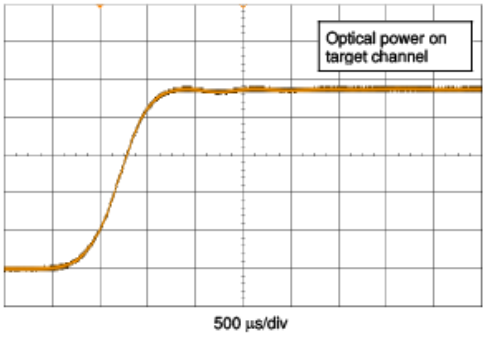

CONTINUOUS SWITCH OPERATION

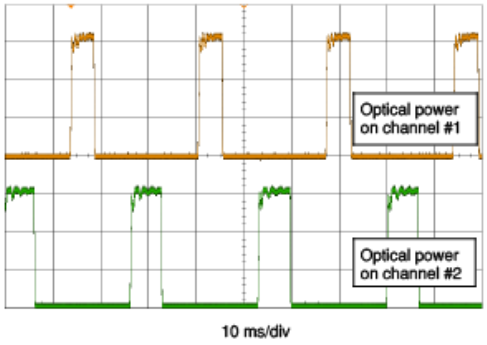

Appendix C

SPECIM FX50

SPECIM FX50

IMPROVE ACCURACY AND REDUCE COSTS

Specim FX50 is a high-speed, accurate and efficient spectral camera specifically designed to industrial environments. It operates on MWIR region and can be used to identify and sort the difficult black plastics, analyze hydrocarbons and minerals, and detect contamination on metal surfaces quickly and reliably.

FEATURES

- Complete spectral camera with compact form factor
- Spectral range of 2.7 – 5.3 µm
- High spatial resolution of 640 pixels
- High image speed of 380 Hz
- Temperature stabilized optics
- Built-in image correction
- Unified spectral calibration between units
- GigE Vision standard interface
- Easy mounting to industrial environment

SPECTRAL RESPONSE

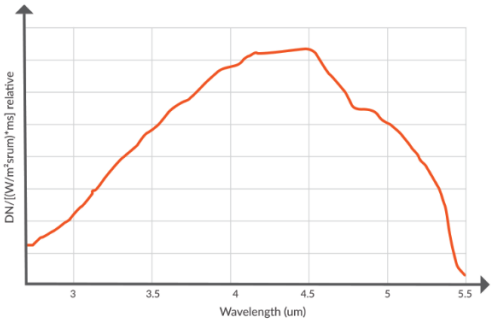

DIMENSIONS

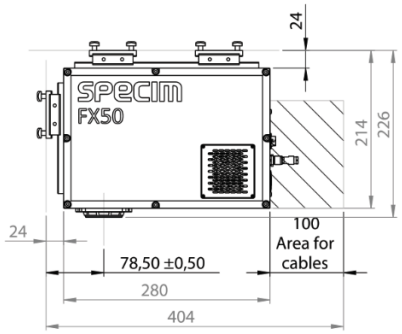

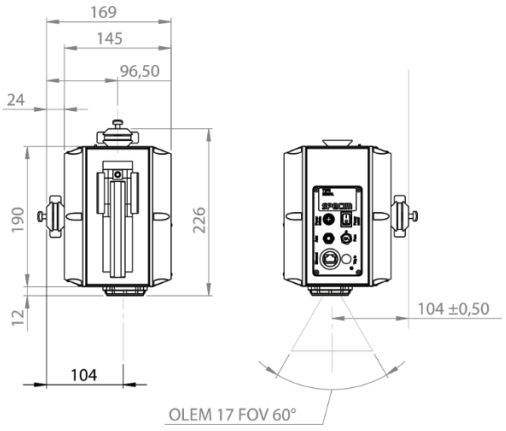

Spectral Range	2.7 - 5.3 µm	
Spectral resolution (FWHM)	35 nm	
Spectral sampling/pixel	8.44 nm	Without binning
Spectral bands	154	With default binning
Numerical aperture	2.0	
Optics magnification	0.5	
Effective pixel size	30 µm	At fore lens image plane
Effective slit width	104 µm	At fore lens image plane
Effective slit length	19.2 mm	At fore lens image plane
Dynamic Range	1600:1 with 1.5 ms exposure time	Usable dynamic range / noise
Spatial samples	640	
Bit depth	16	
Maximum frame rate	380 fps	Full image with default binning
Binning	1,2,4 spectral and spatial	Default: 2 spectral x 1 spatial
ROI	Freely selectable multiple bands of interest	Minimum height of ROI is two 1-binned rows. Maximum frame rate is determined by total number of rows between first row of first mROI and last row of last mROI – not the total number of rows included in the mMROI's.
Pixel operability	Number of operable pixels >99.7% Allowed clusters: Size 4-8 pixels: <= 12 Size 9-12 pixels: 2 Size 13-19 pixels: 1 Size >19 pixels: 0	
Image corrections	Non uniformity correction Bad pixel replacement Automatic Image Enhancement (AIE)	One point NUC AIE: Unified spectral calibration + corrected smile and keystone aberrations
Sensor material	InSb	
Integrated cooler	Stirling	Up to 25000 hours
Full well capacity	5.1 Me-	
Read-out modes	IWR / ITR	
Optics temperature	TEC-stabilized	Default is 20 degrees Celsius
Lens mount	Custom mount	
Fore lens options	OLEM43, OLEM23, OLEM17	
Field of view	24 deg, 45 deg, 60 deg	
Camera digital data output/control interface	GigE Vision, Custom ethernet	
Camera control protocols	GenICam, JSON-RPC	
Power input	24 V DC	
Power consumption	Max 90 W Typical 40 W	During simultaneous cool-down of optics and detector
Connectors	Ethernet Aux - 0306423 (09-0428-90-08) Binder 8pin Power - 0306627 (LF10WBR-4P) Hirose 4pin Trigger in	
IP	IP40	
Dimensions (L x W x H)	280 x 202 x 169 mm	Mounting surface option on three sides. Mounting kit adds 24 mm distance on mounting side.
Weight	7 kg	
Storage temperature	-20 ... +50 °C	
Operating temperature	+5 ... +40 °C	
Relative humidity	5% – 95% (non-condensing)	